Dipartimento Energia

JENDL-3.1 IRON VALIDATION ON THE PCA-REPLICA (H_2O/FE) SHIELDING BENCHMARK EXPERIMENT

M. PESCARINI, M.G. BORGIA
ENEA - Centro Ricerche "Ezio Clementel", Bologna

RT/ERG/97/1

ENTE PER LE NUOVE TECNOLOGIE,
L'ENERGIA E L'AMBIENTE

Dipartimento Energia

JENDL-3.1 IRON VALIDATION ON THE PCA-REPLICA (H_2O/FE) SHIELDING BENCHMARK EXPERIMENT

M. PESCARINI, M.G. BORGIA
ENEA - Centro Ricerche "Ezio Clementel", Bologna

RT/ERG/97/1

Testo pervenuto nel febbraio 1997

RIASSUNTO

L'esperienza benchmark di schermaggio neutronico PCA-REPLICA (H_2O/Fe) e' analizzata usando il codice SN 2-D DOT 3.5-E e il metodo di sintesi 3-D-equivalente del flusso. Questo benchmark ingegneristico riproduce la geometria radiale ex-core di un PWR, incluso un simulatore di recipiente in pressione di reattore (RPV) di acciaio dolce, ed e' dedicato a verificare l'accuratezza di calcolo dei parametri in-vessel di esposizione neutronica (fluenza veloce e tassi di dislocazione del ferro). Questa accuratezza e' fortemente dipendente dalla qualita' delle sezioni d'urto neutroniche del ferro usate per descrivere le reazioni nucleari all'interno del simulatore RPV. In particolare, in questo rapporto, vengono provate le sezioni d'urto basate sui files di dati JENDL-3.1 del ferro, attraverso un confronto dei risultati calcolati integrali e spettrali con i corrispondenti dati sperimentali. Inoltre i presenti risultati sono confrontati, sulla stessa esperienza benchmark, con quelli di una precedente validazione ENEA-Bologna delle sezioni d'urto del ferro ENDF/B VI. Il confronto dei risultati integrali indica che, per tutti i rivelatori a soglia considerati (Rh-103 (n,n') Rh-103m, In-115 (n,n') In-115m e S-32 (n,p) P-32), i dati del ferro naturale JENDL-3.1 producono soddisfacenti risultati simili a quelli ottenuti con i dati del ferro ENDF/B VI. Al contrario, quando si usa il file di dati Fe-56 JENDL-3.1, si ottengono risultati fortemente sottostimati per i rivelatori a piu' bassa energia di soglia, Rh-103 e In-115. Questo fatto, in particolare, diventa piu' evidente al crescere della profondita' della penetrazione neutronica nel simulatore RPV.

SUMMARY

The PCA-REPLICA (H_2O/Fe) neutron shielding benchmark experiment is analysed using the SN 2-D DOT 3.5-E code and the 3-D-equivalent flux synthesis method. This engineering benchmark reproduces the ex-core radial geometry of a PWR, including a mild steel reactor pressure vessel (RPV) simulator, and is designed to test the accuracy of the calculation of the in-vessel neutron exposure parameters (fast fluence and iron displacement rates). This accuracy is strongly dependent on the quality of the iron neutron cross sections used to describe the nuclear reactions within the RPV simulator. In particular, in this report, the cross sections based on the JENDL-3.1 iron data files are tested, through a comparison of the calculated integral and spectral results with the corresponding experimental data. In addition, the present results are compared, on the same benchmark experiment, with those of a preceding ENEA-Bologna validation of the ENDF/B VI iron cross sections. The integral result comparison indicates that, for all the threshold detectors considered (Rh-103 (n,n') Rh-103m, In-115 (n,n') In-115m and S-32 (n,p) P-32), the JENDL-3.1 natural iron data produce satisfactory results similar to those obtained with the ENDF/B VI iron data. On the contrary, when the JENDL-3.1 Fe-56 data file is used, strongly underestimated results are obtained for the lower energy threshold detectors, Rh-103 and In-115. This fact, in particular, becomes more evident with increasing the neutron penetration depth in the RPV simulator.

INDEX

JENDL-3.1 IRON VALIDATION ON THE PCA-REPLICA (H_2O/FE) SHIELDING BENCHMARK EXPERIMENT

1 - INTRODUCTION

The results of a neutron data validation on the PCA-REPLICA (H_2O/Fe) shielding benchmark experiment /1/ are presented in this report. The experiment was carried out in the United Kingdom, at Winfrith, in the ASPIS facility of the NESTOR low-flux experimental reactor. PCA-REPLICA reproduces the ex-core radial geometry of a PWR and is closely related to light water reactor pressure vessel (LWR-PV) safety. In particular, it is designed to test the accuracy of the calculated neutron exposure parameters (fast neutron fluence and iron displacement rates) in a mild steel reactor pressure vessel (RPV) simulator. The LWR-PV transport analysis requires these parameters to be evaluated with the highest possible degree of accuracy in the RPV neutron damage calculations. On the other hand, the precision obtainable in the calculation of these parameters is strongly sensitive to the quality of the iron neutron cross sections used to describe the nuclear reactions within the RPV.
In this report, neutron group cross sections derived from the JENDL-3.1 iron data files are used in discrete ordinates (SN) transport calculations to describe the nuclear reactions within the PCA-REPLICA RPV simulator. These cross sections are tested, in particular, through a comparison of the calculated integral and spectral results with the corresponding experimental data. The calculations employ, as macroscopic cross section working libraries, two 28 neutron energy group problem-dependent libraries, with a group structure similar to those typically used in the practical neutron fluence transport calculations for the LWR-PV dosimetry. The first library contains the JENDL-3.1 natural iron cross sections while the second contains the JENDL-3.1 cross sections for each of the four isotopes of the natural iron.
The present results are compared, in addition, with those of a preceding ENEA-Bologna validation /2/ /3/ of the ENDF/B VI iron cross sections.
This work is based on a JEF document /4/ presented at the JEF Working Group Meetings on Benchmark Testing, Data Processing and Evaluations, held in Issy-les-Moulineaux, at the NEA Data Bank, on July 3-4, 1996.
A summary /5/ of this work was presented in Prague (Czech Republic) at the 9th International Symposium on "Reactor Dosimetry", September 2-6, 1996.

2 - PCA-REPLICA EXPERIMENTAL DETAILS

The PCA-REPLICA experimental facility (see FIGS. 1, 2 and 3) reproduced exactly the 12/13 geometrical configuration of the Oak Ridge (USA) PCA (Pool Critical Assembly) experiment /6/, but for one important feature. The reactor source of the PCA experiment was replaced, in

the PCA-REPLICA experiment, by a thin rectangular fission plate, whose dimensions were 63.5 cm x 40.2 cm x 0.6 cm. The cross-sectional area (63.5 cm x 40.2 cm) of this fission plate was identical to that of the PCA source. In particular, the simpler source configuration of the PCA-REPLICA experiment could more easily be calibrated with a high degree of accuracy. In this way, since a pure neutron fission spectrum distribution can correctly be assumed as the fission plate neutron source in transport calculations, the uncertainties related to the source distribution and strength are reduced. This minimizes the contribution of the source to any eventual difference between the experimental and the calculated integral results.

The fission plate was made of highly enriched uranium (93.0 w% in U-235) alloyed with aluminium. It was irradiated by the NESTOR reactor (30 kW at full power) in the ASPIS shielding facility (see FIG. 2), through a graphite thermal column (total thickness 43.91 cm). Beyond the fission plate, the PCA-REPLICA shielding array was arranged in a large parallelepiped steel tank (square section; side 180.0 cm) filled with water and surrounded by a thick concrete shield (see FIG. 2). After the first water gap (12.1 cm), there was the stainless steel thermal shield (TS) simulator (thickness 5.9 cm) and the second water gap (12.7 cm). Then the mild steel RPV simulator (thickness T = 22.5 cm) was located and tightly connected with a void box made of a thin layer of aluminium, simulating the air cavity (thickness 29.58 cm) between the RPV and the biological shield in a real PWR. The fission plate, the TS, the RPV and the Void Box were perfectly orthogonally aligned and centred along the imaginary line Z (horizontal or nuclear axis), passing through the centre of the fission plate (see FIGS. 3 and 4).

Along this nuclear axis, three types of threshold detectors were located in ten different positions and gave the integral measurements. The detectors used were: Rh-103 (n,n') Rh-103m, In-115 (n,n') In-115m and S-32 (n,p) P-32. The threshold energies are respectively 0.04, 0.34 and 0.95 MeV while the effective threshold energies, in the U-235 fission spectrum, are 0.69, 1.30 and 2.8 MeV (see /7/). It should be noted that the effective threshold is only a rough indicator of the start of the response for the specific detector. If one wishes to characterize the response range more accurately it is preferable to use the median energy of the response and the energy range corresponding to, for example, 90% of the response. The median energy is defined such that, in the specific spectrum, the responses below and above this energy are equal. The energy range corresponding to 90% of the response implies that 5% of the response is to the left hand side and another 5% is to the right hand side of this energy range. In particular the Rh-103, In-115 and S-32 median energies, in the U-235 fission spectrum, are respectively 2.3, 2.6 and 4.0 MeV and the energy ranges corresponding to 90% of the response are respectively 0.72 - 5.8 MeV, 1.1 - 5.9 MeV and 2.3 - 7.3 MeV (see /7/). However, the effective energy threshold parameter may be used to characterize the response energy range of the specific detector, for the sake of simplicity.

The spectral measurements were performed in two positions: at a quarter thickness of the RPV simulator (T/4 position) and in the Void Box. Two kinds of spectrometer were used. Spherical hydrogen-filled proportional counters (SP-2 type; internal diameter 40.0 mm) were employed. Individual counters with gas fillings of approximately 0.5, 1.0, 3.0 and 10.0 atmospheres were used in combination, to cover the energy range from 50.0 keV to 1.2 MeV. The neutron fluxes between 1.0 and 10.0 MeV were determined with a spherical 3.5 ml organic liquid (NE213) scintillator.

Complete experimental details are reported in ref. /1/.

3 - MULTIGROUP LIBRARY AND DATA PROCESSING

The VITAMIN-J /8/ multigroup neutron shielding library, based on the JEF-1 /9/ nuclear data files, is the principal cross section source for the transport calculations. It covers the energy range 1.0E-5 eV - 19.64 MeV with 175 energy groups (see TAB. 1) and contains most of the nuclides required for the description of the PCA-REPLICA mixtures.
Additional JEF-1 cross sections not included in VITAMIN-J, referring to nuclides components of stainless steel, concrete and air are used. These cross sections were produced in the 175 group structure, using the NJOY/THEMIS data processing system (version 1, July 1985, equivalent to NJOY /10/, June 1983 version), based on the Bondarenko /11/ self-shielding factor approach for resonance absorption. The following nuclides (temperature 300 °K ; infinite dilution) were treated: N-14 (MAT 4074), K-nat (MAT 4190), Ti-nat (MAT 4220), Cu-nat (MAT 4290), Nb-93 (MAT 4413) and Mo-nat (MAT 4420).
Along with the above mentioned JEF-1 cross sections, already processed and used in the previous JEF-1 natural iron validation /12/, the JENDL-3.1 natural iron file and the JENDL-3.1 data files for the four iron isotopes are processed with the NJOY data processing system (version 89.62, May 1990) similarly to the ENDF/B VI iron isotopes (see /2/). This version was chosen /13/ in the first JEF sponsored NJOY User Group Meeting (Saclay, NEA Data Bank, September 20, 1991) as the official version for the processing of the JEF-2 data files and it was recommended /14/ as the standard version to produce JEF-2 cross sections for the benchmarking. In particular Fe-nat (MAT 3260), Fe-54 (MAT 3261), Fe-56 (MAT 3262), Fe-57 (MAT 3263) and Fe-58 (MAT 3264) are processed to obtain P5 neutron cross sections in the VITAMIN-J 175 neutron group structure. All the nuclides are processed at the temperature of 300 °K and at the background cross section σ_0 = 1.0E10 barns (infinite dilution). In addition, the Fe-nat and the Fe-56 data files are processed at the same preceding temperature and at σ_0 = 1.0E-6 barns, to obtain totally self-shielded cross sections.
The same threshold detector response functions, obtained from the NEA Data Bank and used in the previous validations of the JEF-1 /12/, JEF-2.1 /15/ and ENDF/B VI /2/ iron data files on PCA-REPLICA, are employed. In particular, the cross sections for the Rh-103 (n,n') Rh-103m, the In-115 (n,n') In-115m and the S-32 (n,p) P-32 reactions were processed at the NEA Data Bank in the VITAMIN-J 175 neutron group structure by using the GROUPIE code /16/. The Rh-103 cross sections were taken from the ACTL-82 dosimetry data file /17/, while the In-115 and S-32 cross sections were obtained from the ENDF/B V nuclear data file.
The preparation of a binary group-independent working library for the ANISN code /18/ is carried out using a version of the TAPEMAKER program modified to read the FIDO free format.

4 - TRANSPORT CALCULATIONS

The transport calculations are performed in the fixed source option with the SN 1-D ANISN and the SN 2-D DOT 3.5-E /19/ codes. The procedure of the calculation is identical to that adopted in refs. /2/, /12/ and /15/.
The plane geometry is used for both the ANISN and DOT 3.5-E codes and the orders of the approximation of the flux angular discretization and of the expansion in Legendre polynomials of the scattering cross section, are respectively S8 and P3 for all the ANISN and DOT 3.5-

E runs. In the DOT 3.5-E calculations, the fully symmetrical S8 quadrature set is employed throughout.
The convergence criterion for the pointwise scalar flux error is 1.0E-4 in ANISN and 1.0E-3 in DOT 3.5-E.
Two ANISN runs are performed to collapse the cross sections (including those derived from the JENDL-3.1 iron data files) from the VITAMIN-J 175 group structure to two 28 group problem-dependent working libraries, containing macroscopic cross sections for the calculations with the DOT 3.5-E code: the first library contains the JENDL-3.1 natural iron cross sections while the second contains the cross sections of the four JENDL-3.1 iron isotopes. In these working libraries (see TAB. 2), there are 26 groups above 0.1 MeV, with an average lethargy width of 0.2.
The collapsed microscopic cross sections for the detector response functions, used in the DOT 3.5-E calculations, are the same as those employed previously in the JEF-1 /12/, JEF-2.1 /15/ and ENDF/B VI /2/ iron validations. It is considered that the use of the JENDL-3.1 instead of the JEF-1, the JEF-2.1 or the ENDF/B VI iron cross sections, induces only negligible differences in the flux weighted detector cross sections in the RPV. This choice assures that any difference between the results of the JENDL-3.1 calculations and those from the JEF-1, the JEF-2.1 or the ENDF/B VI calculations, are attributable only and exclusively to the iron data files. In particular, the details of the detector cross section collapsing are reported in ref. /12/.
Obviously, the material composition and the geometrical model of the PCA-REPLICA experiment, adopted in the present ANISN and DOT 3.5-E calculations, are the same as those used in refs. /2/, /12/ and /15/. The only difference refers to the JENDL-3.1 iron cross sections, used to describe the thermal shield and the pressure vessel simulators.
In particular, in these regions, the totally self-shielded Fe-nat cross sections are used (see 3). Alternatively, the totally self-shielded Fe-56 cross sections are employed, while, for the other remaining iron isotopes, the infinite dilution cross sections are used (see 3). The atomic densities of the iron isotopes are calculated taking the following weight fractions into account, as recommended in ref. /7/: 5.8 w% for Fe-54, 91.72 w% for Fe-56, 2.2 w% for Fe-57 and 0.28 w% for Fe-58. Four collapsed macroscopic cross section sets for the RPV mild steel are obtained from each ANISN run and assigned to the respective equi-spaced zones in DOT 3.5-E, to obtain a better spectral description within the RPV. This is done in both the calculations with the natural iron or, alternatively, with the four distinct iron isotopes.
Concerning the spatial discretization methods, the weighted difference model is used in ANISN while in DOT 3.5-E, in addition, the exponential model /20/ /21/ is employed as well. The latter is particularly suited for large geometry, neutron deep penetration problems and normally requires a shorter calculation time, with respect to the weighted difference model.
No leakage treatment is used in ANISN to collapse the cross sections, while the 3-D-equivalent flux synthesis method is used for the DOT 3.5-E calculations. The method consists in obtaining 3-D-equivalent fluxes from DOT 3.5-E by combining the results from 2-D and 1-D-equivalent calculations in Cartesian coordinates. The following relationship for space, energy and angular dependent flux is used $\Phi(X,Y,Z) = \Phi(X,Z) \times \Phi(Y,Z) / \Phi(Z)$. The use of DOT 3.5-E to calculate $\Phi(Z)$, by inserting appropriate reflection boundary conditions, is preferable to the use of ANISN for this purpose, since the same angular quadrature sets, consistent with the other 2-D calculations, can be employed.
Only the ex-NESTOR-core geometry (see FIG. 3) of the PCA-REPLICA experiment is described in the DOT 3.5-E calculations and as Z is a symmetry axis for the (X,Z) and (Y,Z) planes of the geometrical model (see FIGS. 3 and 4), only half of these planes are considered

with proper boundary conditions. In the 2-D DOT 3.5-E calculations, the reflection option is used to describe the external boundary condition of the side overlapping the Z axis, in the plane spatial region described. The void option is used for the other three sides. In the 1-D-equivalent DOT 3.5-E calculation, a plane spatial region with two sides measuring a unit thickness (1.0 cm) in a direction orthogonal to the Z axis is described. Unlike the 2-D cases, the reflection option is assumed in this calculation not only at the external boundary of the side overlapping the Z axis but also on the opposite side.
The thickness of the mesh intervals in the Z and in the orthogonal X and Y axes is taken such as not to be larger than 1.0 cm in the water and steel zones, as recommended in the standard methodology reported in ref. /22/. The mesh intervals are chosen such that the detectors are found at the midpoint of the corresponding interval. Volumetric sources derived from a pure fission spectrum distribution (see TABS. 1 and 2), obtained at the NEA Data Bank with the NJOY data processing system from the JEF-1 U-235 data file, are used in ANISN and DOT 3.5-E. Since only the ex-NESTOR-core geometry is described in the calculations, the volumetric sources are exclusively assigned to the fission plate mesh interval. The source normalizations are obtained from the fission spectrum data, taking into account that 1 Watt of power corresponds to 3.121E10 fissions/s and the value of $\bar{\nu}$, the average number of neutrons emitted per U-235 fission, is 2.437, as assumed in ref. /1/.
The normalization used for the integral results refers to 1 Watt of NESTOR reactor power while, for the spectral results, refers to 1 Watt of power of the fission plate. The conversion from one normalization to the other is simple since the fission plate power per NESTOR Watt is 6.74E-4 Watt, as deduced from experimental measures in ref. /1/.

5 - DISCUSSION OF THE RESULTS

The threshold detector integral results are reported in the TABS. 3, 4, 5 and 6. In these tables, the total experimental errors are within the confidence level of one standard deviation (1 σ). The total errors are the sums (see /1/) of the random errors due to the counting statistics and of the errors coming from the counter calibration: the latter are 3%, 2% and 4%, respectively for the Rh-103, In-115 and S-32 detectors. Since the "as measured" experimental results (E), in the preceding tables, contain a contribution from the background neutrons coming directly from the NESTOR core while the calculated results (C) refer only to the neutrons produced in the fission plate, the following corrections are introduced: the experimental values (E), in the C/E (Calculated / Experimental) activity ratios, are reduced by 4% in the RPV and Void Box measure positions and by 2% in the water measure positions, as recommended in ref. /1/. These corrections are necessary to permit a consistent comparison between the calculated and the experimental results (see 4).
The TABS. 3 and 4 report a comparison of the results of the JENDL-3.1 natural iron calculations with the results of the ENDF/B VI calculations.
The TABS. 5 and 6 show the preceding results, obtained with the JENDL-3.1 natural iron cross sections, compared with those obtained with the cross sections of the four JENDL-3.1 iron isotopes. The C/E activity ratios are plotted in the FIGS. 5, 6 and 7, respectively, for the Rh-103, In-115 and S-32 detectors. The in-vessel measure positions are at one quarter (T/4 position) and at three quarters (3T/4 position) of the thickness T of the RPV simulator.
The spectral results of the JENDL-3.1 Fe-nat and ENDF/B VI calculations are compared in the FIGS. 8, 9, 10 and 11 while those referring to the JENDL-3.1 and JENDL-3.1 Fe-nat

calculations are shown in the FIGS. 12, 13, 14 and 15. The experimental spectral results are available only in the T/4 and Void Box measure positions (see 2). Unfortunately, the errors associated with the experimental neutron group fluxes are not available (see /1/) and consequently are not indicated in the FIGS. 8, 10, 12 and 14. In these figures, between 0.1 and 10.0 MeV, the experimental neutron group fluxes are reduced by 4%, in both the T/4 and the Void Box measure positions, to correct for the presence of the background neutrons.
All the integral and spectral results presented refer to the calculations using the weighted difference spatial discretization model although calculations with the exponential model are performed as well (see 4). The weighted difference model (see 4) is specifically recommended (see /22/) for the neutron fluence calculations in the LWR-PV dosimetry.

5.1 - Integral Results

The results of the comparison of the DOT 3.5-E transport calculations, employing alternatively the JENDL-3.1 Fe-nat, the JENDL-3.1 or the ENDF/B VI iron cross sections for the description of the thermal shield and RPV simulators, are separately presented for each detector.

5.1.1 - Rh-103 (n,n') Rh-103m Detector

In the in-vessel measure positions, the JENDL-3.1 Fe-nat and the ENDF/B VI calculations give almost equivalent results (see TAB. 3 and FIG. 5) contained within the experimental error range of each detector in the specific measure position. Activity underprediction (about 15%) of the experimental data is still noted in the Void Box position for both the calculations.
In the JENDL-3.1 calculations, the in-vessel results are significantly underpredicted in comparison with the experimental data and this underprediction increases with the neutron penetration depth in the RPV simulator: about 10% in the T/4 position, 20% in the 3T/4 position and up to a dramatic 45% in the Void Box position.

5.1.2 - In-115 (n,n') In-115m Detector

Both the JENDL-3.1 Fe-nat and the ENDF/B VI calculations give results (see TAB. 4 and FIG. 6) that underestimate the experimental activities and this underprediction increases progressively with the neutron penetration depth in the RPV simulator. Nevertheless, the JENDL-3.1 Fe-nat and the ENDF/B VI calculations give almost equivalent results. Thus, the JENDL-3.1 Fe-nat calculations give an underestimate of about 10% in the 3T/4 position and 20% in the Void Box position while the ENDF/B VI calculations give an underestimate of about 15% in the 3T/4 position and 20% in the Void Box position. These results suggest that probably there are still deficiencies with the JENDL-3.1 Fe-nat and the ENDF/B VI iron data files.
About the results of the JENDL-3.1 calculations (see TAB. 6 and FIG. 6), they are all significantly underestimated in comparison with the experimental activities. In the 3T/4 position, for example, there is an underestimate of about 25% while a remarkable 40% is reached in the Void Box.

5.1.3 - S-32 (n,p) P-32 Detector

All the JENDL-3.1 Fe-nat, JENDL-3.1 and ENDF/B VI calculations produce very satisfactory results (see TABS. 4 and 6 and FIG. 7), contained within the error range of each S-32 detector in the specific measure position. All the results are not affected by the trend to an increase in the activity underprediction with the neutron penetration depth in the RPV simulator.

5.2 - Spectral Results

The spectral results are separately discussed for the T/4 and for the Void Box measure positions. The FIGS. 8 and 12 give the spectral trends in the T/4 position while the FIGS. 10 and 14 refer to the Void Box position. The group flux ratios (JENDL-3.1 Fe-nat / ENDF/B VI), obtained from the JENDL-3.1 Fe-nat and the ENDF/B VI calculations, are presented in the FIGS. 9 and 11 for the T/4 and Void Box positions respectively, while the group flux ratios (JENDL-3.1 / JENDL-3.1 Fe-nat), from the JENDL-3.1 and the JENDL-3.1 Fe-nat calculations, are shown in the FIGS. 13 and 15 for the same preceding positions respectively.

5.2.1 - T/4 Measure Position

The JENDL-3.1 Fe-nat and the ENDF/B VI calculations give results rather similar in the T/4 position. The spectral distributions and their ratio, respectively shown in the FIGS. 8 and 9, confirm that both the calculations are particularly in agreement above 0.3 MeV (see FIG. 9). This fact is consistent with the good agreement in the comparison (see 5.1 and FIGS. 5, 6 and 7) of the integral results obtained for all the detectors considered (Rh-103, In-115 and S-32), which have all their effective energy thresholds above 0.3 MeV.
The spectral results of the JENDL-3.1 calculations show a strong flux overestimate in the 0.1 - 0.25 MeV energy range, with respect to both the experimental data (see FIG. 12) and the results of the JENDL-3.1 Fe-nat calculations (see FIGS. 12 and 13). This fact does not influence the corresponding comparison of the integral results in the T/4 position (see FIGS. 5, 6, and 7), since all the detector effective energy thresholds are at higher energies.

5.2.2 - Void Box Measure Position

In the Void Box measure position, the spectral distributions obtained from the JENDL-3.1 Fe-nat and the ENDF/B VI calculations represent acceptable results, although on average, approximately in the energy range 0.1 - 2.0 MeV, a certain trend to underestimate the experimental data is present for both the spectral distributions (see FIG. 10). The flux underestimate in the JENDL-3.1 Fe-nat calculations seems more pronounced and this is more evident in the group flux ratios of the preceding spectral results reported in FIG. 11. The consistency with the integral results is assured also in this case. In fact the Rh-103 and In-115 detectors, having their effective energy thresholds well below 2.0 MeV, underpredict the experimental results (see 5.1 and FIGS. 5 and 6) in both the calculations, while, the calculated results (see 5.1 and FIG. 7) are very satisfactory for the S-32 detector, with an effective energy threshold well above 2.0 MeV.
A comparison of the spectral results of the JENDL-3.1 and JENDL-3.1 Fe-nat calculations with the experimental spectrum is shown in FIG. 14. The JENDL-3.1 calculations produce

strongly underestimated group fluxes, approximately in the energy range 0.25 - 2.5 MeV. This is evident not only with respect to the experimental data but also in comparison with the results of the JENDL-3.1 Fe-nat calculations, as it can be seen in FIG. 15. The flux underestimate of the JENDL-3.1 calculations is remarkable with respect to the group fluxes of the JENDL-3.1 Fe-nat calculations: it reaches a maximum of about 60% at 0.7 MeV and exceeds 40% at 1.0 MeV. Moreover, as in the case of the T/4 position, the results of the JENDL-3.1 calculations below 0.25 MeV are excessively overestimated, with respect to the results of the JENDL-3.1 Fe-nat calculations. The comparison of the spectral results is consistent with the Void Box integral results in the JENDL-3.1 calculations (see 5.1). In fact the calculated activities of the lower effective energy threshold detectors (see FIG. 5 for Rh-103 and FIG. 6 for In-115) strongly (over 40%) underpredict the experimental data while the S-32 calculated activity (see FIG. 7) is satisfactory as for the previous corresponding results of the JENDL-3.1 Fe-nat and ENDF/B VI calculations.

5.3 - Final Comments

As for the comparison of the JENDL-3.1 Fe-nat and ENDF/B VI calculations, it is outlined that, for all the threshold detectors considered (Rh-103, In-115 and S-32), the integral results give values which are almost equivalent for both the calculations. The Rh-103 and S-32 in-vessel results are now within the range of the total experimental error for the specific detector position in both the calculations, while, in the Void Box position, a certain underestimate persists in the Rh-103 results of both the calculations. The In-115 calculated activities of both the calculations are not completely satisfactory since they underpredict the experimental activities, in particular in the 3T/4 position and in the Void Box position. The spectral results in the T/4 and Void Box positions are consistent with the corresponding integral results and are in a fairly good agreement with the experimental spectra.
Concerning the comparison of the JENDL-3.1 and JENDL-3.1 Fe-nat calculations, remarkable discrepancies emerge below about 2.5 MeV, in the spectral results of both the T/4 and Void Box positions. The spectral distributions of both the calculations are almost equivalent above this energy value in both the measure positions and this fact determines directly the consistent integral results of the S-32 detector in the in-vessel and Void Box positions. The S-32 results are in fact within the range of the total experimental error for the specific detector position in both the calculations and in all the measure positions. This is due to the value (2.8 MeV) of the effective energy threshold of the S-32 detector which is above the upper limit (about 2.5 MeV) of the energy region where the spectral discrepancies between the two calculations are evident. On the contrary, in both the measure positions, the spectral results of the JENDL-3.1 calculations are excessively overestimated in the energy range 0.1 - 0.25 MeV, with respect to the results of the JENDL-3.1 Fe-nat calculations. This fact does not influence the integral results of the JENDL-3.1 calculations since the effective energy thresholds of the detectors used are well above 0.25 MeV. Finally, the spectral results of the JENDL-3.1 calculations remarkably underpredict the experimental data and the corresponding spectral results of the JENDL-3.1 Fe-nat calculations in the Void Box position, approximately in the energy range 0.25 - 2.5 MeV. This deep flux underestimate influences, in particular, the results of the lower effective energy threshold detectors. In fact the Rh-103 and In-115 detectors, having their effective energy thresholds respectively at 0.69 and 1.30 MeV, give results strongly underestimated in the Void Box position in comparison with the experimental activities and

the corresponding results of the JENDL-3.1 Fe-nat calculations. These integral results can be better understood considering that the median energies (see 2) of the Rh-103 and In-115 detectors are respectively 2.3 and 2.6 MeV and this roughly means that the strong flux underestimate, up to about 2.5 MeV, influences half of the neutrons which potentially determine the calculated activities of both the detectors.
A possible explanation of the very different results obtained with the JENDL-3.1 and the JENDL-3.1 Fe-nat calculations could be connected with the different evaluations of the iron data files. In the JENDL-3.1 Fe-nat data file, below 4.0 MeV, experimental data for the total cross section were adopted from a work /23/ of A.D. Carlson and R.J. Cerbone. On the contrary, in the JENDL-3.1 Fe-56 data file, the total cross section above 0.250 MeV is obtained with spherical optical model calculations, using the CASTHY code /24/. As it can be observed in FIG. 16, below about 2.5 MeV, the total cross section of the JENDL-3.1 Fe-56 data file appears too much overestimated in comparison with the corresponding values of the JENDL-3.1 Fe-nat data file. This induces more neutrons scattered below the Rh-103 and In-115 effective thresholds (0.69 MeV for Rh-103 and 1.30 MeV for In-115), with respect to the results obtained with the JENDL-3.1 Fe-nat data file. Consequently, this fact involves the Rh-103 and In-115 activity underpredictions in the JENDL-3.1 calculations.
To this purpose, it is interesting to note that strong flux underestimates (see FIG. 17), between 1.0 MeV and about 2.0 MeV, were found as well in a South Korean work /25/ on PWR benchmark calculations, using the JENDL-3.1 Fe-56 cross sections to describe the neutron interactions in the RPV. These flux underestimates are shown not only in comparison with the corresponding results of the calculations using the ENDF/B VI iron data but also in comparison with the calculations using the older ENDF/B IV natural iron data. For example, the flux underestimate in the centre of the cavity (between the RPV and the concrete reactor shield) reaches approximately 60% at about 1.0 MeV, in comparison with the corresponding results of the ENDF/B VI and ENDF/B IV calculations. This value seems to be in agreement with both the previously described spectral and integral results of the JENDL-3.1 calculations in the Void Box position. This connection is consistent since the Void Box is a cavity beyond the PCA-REPLICA pressure vessel simulator and similar spectral shapes should be reproduced with respect to a real PWR cavity. The group flux ratios in the Void Box position, between the spectral results of the JENDL-3.1 and ENDF/B VI calculations, is reported in FIG. 18, to perform a consistent comparison with FIG. 17 which, nevertheless, shows a different normalization. In both the present and the South Korean calculations using the JENDL-3.1 Fe-56 iron cross sections, important flux underestimates with very similar spectral trends are approximately obtained in the energy range 1.0 - 2.0 MeV, with respect to the corresponding results of the ENDF/B VI calculations.
Considering now the most recent Japanese iron files, it is worth of note that the values of the total cross section above 0.250 MeV, in the JENDL-3.2 Fe-56 evaluation, maintain the same values of the corresponding data obtained in the JENDL-3.1 Fe-56 data file. In this way, it was decided to maintain, as a standard reference, the total cross section values, obtained through spherical optical model calculations with the CASTHY code. On the other hand, the values of the inelastic scattering cross section of the JENDL-3.2 Fe-56 data file (see FIG. 19) are rather different from the corresponding values of the JENDL-3.1 Fe-56 data file and this fact could induce rather different results in deep penetration neutron transport calculations. In any case, it is outlined that also the total cross section values of the JENDL-3.2 Fe-56 data file appear (see FIG. 20) strongly overestimated with respect to the corresponding total cross section values of the JENDL-3.1 and JENDL-3.2 natural iron files, between 0.250 MeV (the upper energy limit of the resolved resonance region) and about 2.5 MeV. To this purpose, in

the preceding energy range, it is observed (see FIG. 21) that the JENDL-3.2 Fe-nat total cross section values are only slightly different, in comparison with the corresponding JENDL-3.1 Fe-nat values.

6 - CONCLUSION

The PCA-REPLICA engineering benchmark shielding experiment has been analysed using the SN 2-D DOT 3.5-E code and the 3-D-equivalent flux synthesis method. In particular, totally self-shielded group cross sections of the JENDL-3.1 Fe-nat data file, or alternatively, of the JENDL-3.1 Fe-56 data file have been used to describe the nuclear reactions within a mild steel RPV simulator. The results of this validation have been compared with the results of similar ENEA-Bologna calculations /2/ on PCA-REPLICA, using the ENDF/B VI iron cross sections. It is outlined that, from the comparison of the spectral and integral data, the results of the calculations using the JENDL-3.1 Fe-nat and the ENDF/B VI iron cross sections are in fairly good agreement with the experimental data.
On the contrary, the calculations using the JENDL-3.1 Fe-56 cross sections give results, particularly in the Void Box measure position, severely underestimated in the energy range 0.25 - 2.5 MeV and excessively overestimated in the energy range 0.1 - 0.25 MeV with respect to both the experimental data and the results of the JENDL-3.1 Fe-nat calculations. The present results and those obtained from transport calculations /25/ in the cavity of a real PWR seem to suggest that the use of the JENDL-3.1 Fe-56 cross sections should be carefully considered since they could induce important underpredictions in LWR pressure vessel fast neutron fluence (above 0.1 and 1.0 MeV) and/or radial shielding calculations. The possible cause of the discrepancies between the JENDL-3.1 and the JENDL-3.1 Fe-nat calculations in the present work could be the overestimated total cross section of the JENDL-3.1 Fe-56 data file between 0.250 and about 2.5 MeV, obtained through spherical optical model calculations.
It is worth of note that, the values of the total cross section above 0.250 MeV in the JENDL-3.2 Fe-56 evaluation maintain the same values of the corresponding data obtained from the JENDL-3.1 Fe-56 data file. On the other hand, the values of the inelastic scattering cross section of the JENDL-3.2 Fe-56 data file are rather different from the corresponding values of the JENDL-3.1 Fe-56 data file and this fact could induce different results in deep penetration neutron transport calculations. Finally, it could be interesting to test if the JENDL-3.2 Fe-56 cross sections permit to obtain improved results in shielding benchmark calculations with respect to the JENDL-3.1 Fe-56 cross sections.

ACKNOWLEDGEMENTS

The authors wish particularly to thank G.C. Panini (ENEA-Bologna) for the use of the NJOY data processing system and the COMPLOT graphic program.
Many thanks to E. Sartori (OECD/NEA Data Bank, Issy-les-Moulineaux) for the release of the threshold detector cross sections and fission spectrum data.

REFERENCES

/1/ J. Butler, M.D. Carter, I.J. Curl, M.R. March, A.K. McCracken, M.F. Murphy, A. Packwood, The PCA Replica Experiment PART I, Winfrith Measurements and Calculations, AEEW-R 1736, 1984.

/2/ M. Pescarini, ENDF/B VI IRON VALIDATION ON THE PCA-REPLICA (H_2O/FE) SHIELDING BENCHMARK EXPERIMENT, ENEA Technical Report, RT/INN/94/11, May 1994.

/3/ M. Pescarini, PCA-REPLICA SHIELDING BENCHMARK: FINAL COMPARISON OF THE VALIDATIONS OF THE ENDF/B VI AND JEF-2.1 IRON CROSS SECTION SETS, JEF/DOC-392, JEF Working Group Meetings on Benchmark Testing, Data Processing and Evaluations, NEA Data Bank, Issy-les-Moulineaux, December 9-10, 1992.

/4/ M. Pescarini, M.G. Borgia, PCA-REPLICA SHIELDING BENCHMARK: FINAL COMPARISON OF THE VALIDATIONS OF THE JENDL-3.1 AND ENDF/B VI IRON CROSS SECTION SETS, JEF/DOC-581, JEF Working Group Meetings on Benchmark Testing, Data Processing and Evaluations, NEA Data Bank, Issy-les-Moulineaux, July 3-4, 1996.

/5/ M. Pescarini, JENDL-3.1 AND ENDF/B VI IRON VALIDATION ON THE (H_2O/FE) PCA-REPLICA SHIELDING BENCHMARK, Proceedings of the International Symposium on "Reactor Dosimetry", Prague, Czech Republic, September 2-6, 1996 (to be published).

/6/ W.N. McElroy Editor, LWR PRESSURE VESSEL SURVEILLANCE DOSIMETRY IMPROVEMENT PROGRAM: PCA EXPERIMENTS AND BLIND TEST, HEDL-TME 80-87, NUREG/CR-1861, 1981.

/7/ J.H. Baard, W.L. Zijp, H.J. Nolthenius, Nuclear Data Guide for Reactor Neutron Metrology, Kluyver Academic Press, Dordrecht, 1989.

/8/ E. Sartori, VITAMIN-J, a 175 group neutron cross section library based on JEF-1 for shielding benchmark calculations. NEA DATA BANK, JEF/DOC-100 Preliminary, 1985.

/9/ INDEX TO THE JEF-1 NUCLEAR DATA LIBRARY, VOLUME I, GENERAL PURPOSE FILE, JEF REPORT 1, OECD-NEA DATA BANK, July 1985.

/10/ R.E. MacFarlane, D.W. Muir, R.M. Boicourt, The NJOY Nuclear Data Processing System, LA-9303-M: Vol. I and II, 1982; Vol. III, 1987.

/11/ I.I. Bondarenko, M.N. Nikolaev, L.P. Abagyan, N.O. Bazaziants, Group Constants for Nuclear Reactors Calculations, published by Consultants Bureau, New York, 1964.

/12/ M. Pescarini, DOT 3.5-E (DOT 3.5-E/JEF-1) ANALYSIS OF THE PCA-REPLICA (H_2O/FE) SHIELDING BENCHMARK FOR THE LWR-PV DAMAGE PREDICTION, ENEA Technical Report, RT/INN/90/21, October 1990.

/13/ Summary Record of the JEF Working Groups on Data Processing, Benchmark Testing and Evaluations, JEF/DOC-369, NEA Data Bank, Saclay, December 4-5, 1991.

/14/ E. Fort, PROPOSALS FOR JEF2 VALIDATION, JEF/DOC-296, Cadarache, October 1991.

/15/ M. Pescarini, F. Fabbri, JEF-2.1 IRON VALIDATION ON THE PCA-REPLICA (H_2O/FE) SHIELDING BENCHMARK EXPERIMENT, ENEA Technical Report, RT/INN/93/44, December 1993.

/16/ D.E. Cullen, Program GROUPIE (version 79-1): calculation of Bondarenko self-shielded neutron cross sections and multiband parameters from data in the ENDF/B format, UCRL-50400, Vol. 17, Part D, July 4, 1980.

/17/ M.A. Gardner, R.J. Howerton, ACTL: Evaluated Neutron Activation Cross Section Library, Evaluation Techniques and Reaction Index, UCRL-50400, Vol. 4, Rev. 1, October 17, 1978.

/18/ W.W. Engle, jr., A Users Manual for ANISN. One Dimensional Discrete Ordinates Transport Code with Anisotropic Scattering. Union Carbide Nuclear Division, Oak Ridge K-1693. Updated: June 6, 1973.

/19/ W.A. Rhoades, F.R. Mynatt, THE DOT III TWO-DIMENSIONAL DISCRETE ORDINATES TRANSPORT CODE, ORNL-TM-4280, September 1973; W.A. Rhoades, Comments on the DOT 3.5 Version of DOT III, Nov. 1975; DOT 3.5-E version, released February 28, 1977.

/20/ P.Barbucci, F. Di Pasquantonio, IMPLEMENTATION OF THE EXPONENTIAL SUPPLEMENTARY EQUATIONS ON DOT III AND DOT 3.5 CODES, ENEL-CRTN, Milano, Italy, 1977.

/21/ P. Barbucci, F. Di Pasquantonio, Exponential Supplementary Equations for SN Methods: the Two-Dimensional Case, Paper P.II.-1 presented at V International Conference on Reactor Shielding, Knoxville, Tenn. USA, April 18-23, 1977.

/22/ F.B.K. Kam, R.E. Maerker, M.L. Williams, F.W. Stallmann, Pressure Vessel Fluence Analysis and Neutron Dosimetry, ORNL/TM-10651, NUREG/ CR-5049, Oak Ridge, December 1987.

/23/ A.D. Carlson, R.J. Cerbone, High Resolution Measurements of the Total Neutron Cross Sections of Nitrogen and Iron, Nuclear Science and Engineering, Vol. 42, pp. 28-40, 1970.

/24/ S. Igarasi, Journal of Nuclear Science and Technology, Vol. 12, p. 67, 1975.

/25/ Jung-Do Kim, Choong-Sup Gil, APPLICATIONS OF ENDF/B-VI AND JENDL-3.1 IRON DATA TO REACTOR PRESSURE VESSEL FLUENCE ANALYSIS USING CONTINUOUS ENERGY MONTE CARLO CODE MCNP, Proceedings of the International Conference "Nuclear Data for Science and Technology", Vol. II, pp. 1003-1005, Gatlinburg, Tennessee, USA, May 9-13, 1994.

TABLES

TAB. 1

VITAMIN-J 175 NEUTRON GROUP STRUCTURE AND U-235 JEF-1

FISSION SPECTRUM USED IN ANISN CALCULATIONS

Group	Upper Energy (eV)	Lethargy Width	Fission Spectrum
1	1.964030E+07	0.1250	3.248388E-06
2	1.733250E+07	0.0250	1.398165E-06
3	1.690461E+07	0.0250	1.936392E-06
4	1.648720E+07	0.0500	6.263816E-06
5	1.568310E+07	0.0500	1.133665E-05
6	1.491830E+07	0.0250	8.576016E-06
7	1.454990E+07	0.0250	1.124797E-05
8	1.419070E+07	0.0250	1.463924E-05
9	1.384030E+07	0.0250	1.889525E-05
10	1.349860E+07	0.0500	5.500691E-05
11	1.284000E+07	0.0250	3.880591E-05
12	1.252320E+07	0.0250	4.864985E-05
13	1.221400E+07	0.0500	1.353004E-04
14	1.161830E+07	0.0500	2.037325E-04
15	1.105170E+07	0.0500	2.991341E-04
16	1.051270E+07	0.0500	4.286927E-04
17	1.000000E+07	0.0500	6.004737E-04
18	9.512310E+06	0.0500	8.230745E-04
19	9.048390E+06	0.0500	1.105174E-03
20	8.607100E+06	0.0500	1.455316E-03
21	8.187330E+06	0.0500	1.880966E-03
22	7.788030E+06	0.0500	2.389141E-03
23	7.408200E+06	0.0500	2.984727E-03
24	7.046900E+06	0.0500	3.670641E-03
25	6.703220E+06	0.0167	1.392379E-03
26	6.592390E+06	0.0333	3.055182E-03
27	6.376290E+06	0.0500	5.312603E-03
28	6.065320E+06	0.0500	6.262045E-03
29	5.769510E+06	0.0500	7.287778E-03
30	5.488130E+06	0.0500	8.380435E-03
31	5.220470E+06	0.0500	9.527788E-03
32	4.965860E+06	0.0500	1.071522E-02
33	4.723680E+06	0.0500	1.192939E-02
34	4.493300E+06	0.1000	2.751900E-02
35	4.065710E+06	0.1000	3.227513E-02
36	3.678800E+06	0.1000	3.666446E-02
37	3.328720E+06	0.0500	1.980929E-02
38	3.166380E+06	0.0500	2.067987E-02
39	3.011940E+06	0.0500	2.144936E-02
40	2.865050E+06	0.0500	2.211976E-02
41	2.725320E+06	0.0500	2.268421E-02
42	2.592400E+06	0.0500	2.313813E-02
43	2.465970E+06	0.0333	1.560800E-02
44	2.385210E+06	0.0084	3.958896E-03

TAB. 1 (Continued)

Group	Upper Energy (eV)	Lethargy Width	Fission Spectrum
45	2.365250E+06	0.0083	3.917221E-03
46	2.345700E+06	0.0167	7.900245E-03
47	2.306860E+06	0.0333	1.582282E-02
48	2.231300E+06	0.0500	2.385848E-02
49	2.122480E+06	0.0500	2.389148E-02
50	2.018970E+06	0.0500	2.383137E-02
51	1.920500E+06	0.0500	2.367743E-02
52	1.826840E+06	0.0500	2.344405E-02
53	1.737740E+06	0.0500	2.313087E-02
54	1.652990E+06	0.0500	2.275067E-02
55	1.572370E+06	0.0500	2.230541E-02
56	1.495690E+06	0.0500	2.181110E-02
57	1.422740E+06	0.0500	2.126611E-02
58	1.353350E+06	0.0500	2.068008E-02
59	1.287350E+06	0.0500	2.006566E-02
60	1.224560E+06	0.0500	1.941920E-02
61	1.164840E+06	0.0500	1.875573E-02
62	1.108030E+06	0.1000	3.545629E-02
63	1.002590E+06	0.0417	1.397063E-02
64	9.616420E+05	0.0583	1.872289E-02
65	9.071820E+05	0.0500	1.530903E-02
66	8.629380E+05	0.0500	1.462470E-02
67	8.208520E+05	0.0500	1.394998E-02
68	7.808190E+05	0.0500	1.328782E-02
69	7.427380E+05	0.0500	1.264001E-02
70	7.065140E+05	0.0500	1.200828E-02
71	6.720570E+05	0.0500	1.139431E-02
72	6.392810E+05	0.0500	1.079972E-02
73	6.081030E+05	0.0500	1.022509E-02
74	5.784450E+05	0.0500	9.671032E-03
75	5.502330E+05	0.0500	9.137537E-03
76	5.233980E+05	0.0500	8.625790E-03
77	4.978720E+05	0.1000	1.580380E-02
78	4.504930E+05	0.1000	1.401375E-02
79	4.076230E+05	0.0500	6.387535E-03
80	3.877430E+05	0.0500	6.001860E-03
81	3.688330E+05	0.1000	1.092633E-02
82	3.337340E+05	0.1000	9.612545E-03
83	3.019750E+05	0.0116	1.036660E-03
84	2.984920E+05	0.0043	3.800131E-04
85	2.972120E+05	0.0091	7.982298E-04
86	2.945180E+05	0.0250	2.142525E-03
87	2.872480E+05	0.0500	4.081085E-03
88	2.732370E+05	0.1000	7.393822E-03
89	2.472350E+05	0.0500	3.342224E-03
90	2.351770E+05	0.0500	3.124291E-03
91	2.237080E+05	0.0500	2.920048E-03
92	2.127970E+05	0.0500	2.727557E-03

TAB. 1 (Continued)

Group	Upper Energy (eV)	Lethargy Width	Fission Spectrum
93	2.024190E+05	0.0500	2.547189E-03
94	1.925470E+05	0.0500	2.378008E-03
95	1.831560E+05	0.0500	2.219100E-03
96	1.742240E+05	0.0500	2.070629E-03
97	1.657270E+05	0.0500	1.931433E-03
98	1.576440E+05	0.0500	1.800871E-03
99	1.499560E+05	0.0500	1.679167E-03
100	1.426420E+05	0.0500	1.564856E-03
101	1.356860E+05	0.0500	1.458445E-03
102	1.290680E+05	0.0500	1.358644E-03
103	1.227730E+05	0.0500	1.265253E-03
104	1.167860E+05	0.0500	1.178453E-03
105	1.110900E+05	0.1250	2.601804E-03
106	9.803681E+04	0.1250	2.174149E-03
107	8.651712E+04	0.0475	7.287643E-04
108	8.250362E+04	0.0371	5.353556E-04
109	7.949881E+04	0.0991	1.296623E-03
110	7.199819E+04	0.0663	7.688284E-04
111	6.737950E+04	0.1750	1.705777E-03
112	5.656230E+04	0.0750	6.075946E-04
113	5.247530E+04	0.1250	8.752996E-04
114	4.630930E+04	0.1250	7.283422E-04
115	4.086780E+04	0.1750	8.185001E-04
116	3.430680E+04	0.0750	2.909480E-04
117	3.182790E+04	0.1104	3.736077E-04
118	2.850110E+04	0.0541	1.619238E-04
119	2.700020E+04	0.0355	9.944287E-05
120	2.605840E+04	0.0500	1.314222E-04
121	2.478760E+04	0.0250	6.216692E-05
122	2.417550E+04	0.0250	5.989254E-05
123	2.357860E+04	0.0750	1.668622E-04
124	2.187490E+04	0.1250	2.399271E-04
125	1.930450E+04	0.2500	3.646035E-04
126	1.503440E+04	0.2500	2.511861E-04
127	1.170880E+04	0.1000	7.701784E-05
128	1.059460E+04	0.1500	9.597051E-05
129	9.118840E+03	0.2500	1.190496E-04
130	7.101750E+03	0.2500	8.192513E-05
131	5.530852E+03	0.2500	5.635351E-05
132	4.307430E+03	0.1500	2.496621E-05
133	3.707450E+03	0.1000	1.378541E-05
134	3.354640E+03	0.1000	1.186758E-05
135	3.035400E+03	0.1000	1.021613E-05
136	2.746540E+03	0.0500	4.562346E-06
137	2.612600E+03	0.0500	4.233721E-06
138	2.485170E+03	0.1000	7.570824E-06
139	2.248670E+03	0.1000	6.517320E-06
140	2.034680E+03	0.2500	1.259381E-05

TAB. 1 (Continued)

Group	Upper Energy (eV)	Lethargy Width	Fission Spectrum
141	1.584610E+03	0.2500	8.656533E-06
142	1.234100E+03	0.2500	5.951216E-06
143	9.611179E+02	0.2500	4.089942E-06
144	7.485200E+02	0.2500	2.810544E-06
145	5.829480E+02	0.2500	1.931165E-06
146	4.540000E+02	0.2500	1.326756E-06
147	3.535759E+02	0.2500	9.114154E-07
148	2.753640E+02	0.2500	6.259758E-07
149	2.144540E+02	0.2500	4.299103E-07
150	1.670170E+02	0.2500	2.951849E-07
151	1.300730E+02	0.2500	2.025865E-07
152	1.013010E+02	0.2500	1.389780E-07
153	7.889340E+01	0.2500	9.631225E-08
154	6.144220E+01	0.2500	6.619018E-08
155	4.785130E+01	0.2500	4.549100E-08
156	3.726660E+01	0.2500	3.126599E-08
157	2.902330E+01	0.2500	2.149277E-08
158	2.260330E+01	0.2500	1.477111E-08
159	1.760350E+01	0.2500	1.015184E-08
160	1.370960E+01	0.2500	6.977029E-09
161	1.067700E+01	0.2500	4.794828E-09
162	8.315310E+00	0.2500	3.295364E-09
163	6.475970E+00	0.2500	2.264827E-09
164	5.043490E+00	0.2500	1.556839E-09
165	3.927870E+00	0.2500	1.070031E-09
166	3.059030E+00	0.2500	7.354068E-10
167	2.382370E+00	0.2500	5.054162E-10
168	1.855390E+00	0.2500	3.473493E-10
169	1.444980E+00	0.2500	2.387199E-10
170	1.125350E+00	0.2500	1.640609E-10
171	8.764270E-01	0.2500	1.127653E-10
172	6.825610E-01	0.2500	7.751325E-11
173	5.315790E-01	0.2500	5.327232E-11
174	4.139950E-01	1.4207	1.031767E-10
175	1.000010E-01	9.2103	1.389797E-11

Lower Boundary 1.000010E-05

TAB. 2

REDUCED 28 GROUP STRUCTURE AND U-235 JEF-1 FISSION SPECTRUM

USED IN DOT CALCULATIONS

Group	Upper Energy (eV)	Lethargy Width	Fission Spectrum
1	1.964030E+07	0.275	2.418341E-05
2	1.491830E+07	0.200	1.958211E-04
3	1.221400E+07	0.200	1.066860E-03
4	1.000000E+07	0.200	3.984038E-03
5	8.187330E+06	0.200	1.092547E-02
6	6.703220E+06	0.200	2.330998E-02
7	5.488130E+06	0.200	4.055276E-02
8	4.493300E+06	0.200	5.979409E-02
9	3.678800E+06	0.200	7.715350E-02
10	3.011940E+06	0.200	8.939130E-02
11	2.465970E+06	0.200	9.495700E-02
12	2.018970E+06	0.200	9.408360E-02
13	1.652990E+06	0.200	8.813310E-02
14	1.353350E+06	0.200	7.892060E-02
15	1.108030E+06	0.200	6.814970E-02
16	9.071820E+05	0.200	5.717140E-02
17	7.427380E+05	0.200	4.684220E-02
18	6.081030E+05	0.200	3.765930E-02
19	4.978720E+05	0.200	2.981750E-02
20	4.076230E+05	0.200	2.331570E-02
21	3.337340E+05	0.200	1.805090E-02
22	2.732370E+05	0.200	1.386020E-02
23	2.237080E+05	0.200	1.057270E-02
24	1.831560E+05	0.200	8.021900E-03
25	1.499560E+05	0.200	6.061000E-03
26	1.227730E+05	0.100	2.443600E-03
27	1.110900E+05	12.775	1.558960E-02
28	4.139950E-01	10.631	1.170747E-10

Lower Boundary 1.000010E-05

TAB. 3

SUMMARY OF MEASURED AND CALCULATED ^{103}Rh (n,n') ACTIVITIES (*)

ALONG THE NUCLEAR AXIS FOR THE PCA-REPLICA SLAB GEOMETRY BENCHMARK

Detec. Pos.	Dist. from Fiss. Plate (cm)	(1) Measured (E) and Total Error (1 σ)	JENDL-3.1 Natural Iron File		ENDF/B VI Iron Files		Ref. Location
			Calculated (C) DOT 3.5-E (X,Y,Z) Synthesis	(1) C/E	Calculated (C) DOT 3.5-E (X,Y,Z) Synthesis	(1) C/E	
			Weighted Difference Model				
1	1.91	1.69-20 (**) 6.0%	1.42-20	0.86	1.42-20	0.86	
2	7.41	3.78-21 6.0%	3.37-21	0.91	3.37-21	0.91	12 cm Water Gap
3	12.41	1.40-21 6.0%	1.22-21	0.89	1.22-21	0.89	
4	14.01	1.27-21 6.0%	1.09-21	0.88	1.09-21	0.88	
5	19.91	4.23-22 6.0%	3.39-22	0.82	3.41-22	0.82	
6	25.41	1.15-22 7.0%	1.00-22	0.88	1.00-22	0.88	13 cm Water Gap
7	30.41	4.73-23 7.0%	4.06-23	0.88	4.01-23	0.86	
8	39.01	2.07-23 4.0%	1.93-23	0.97	1.91-23	0.96	RPV (1/4 T)
9	49.61	5.53-24 4.9%	5.33-24	1.00	5.40-24	1.02	(3/4 T)
10	58.61	1.80-24 4.6%	1.41-24	0.82	1.51-24	0.87	Void Box

(1) Experimental results contain a contribution from the NESTOR core background. Calculated results refer only to the neutrons produced in the fission-plate for 1 Watt of NESTOR power. As indicated in ref. /1/, E values, in C/E ratios, are reduced by 4 % in the RPV and Void Box and by 2 % in the water.

(*) Saturated activities are in units of reactions/(s.atom.NESTOR Watt). The effective threshold energy for the Rhodium detector is 0.69 MeV.

(**) Read as 1.69×10^{-20} (+/- 6.0%).

TAB. 4

SUMMARY OF MEASURED AND CALCULATED ^{115}In (n,n') AND ^{32}S (n,p) ACTIVITIES (*)

ALONG THE NUCLEAR AXIS FOR THE PCA-REPLICA SLAB GEOMETRY BENCHMARK

Detec. Pos.	Dist. from Fiss. Plate (cm)	(1) Measured (E) and Total Error (1 σ)	JENDL-3.1 Natural Iron File		ENDF/B VI Iron Files		Ref. Location
			Calculated (C) DOT 3.5-E (X,Y,Z) Synthesis	(1) C/E	Calculated (C) DOT 3.5-E (X,Y,Z) Synthesis	(1) C/E	
			Weighted Difference Model				
		Indium Activities					
8	39.01	(**) 3.93-24 2.9%	3.55-24	0.94	3.45-24	0.92	RPV (1/4 T)
9	49.61	8.23-25 3.4%	7.03-25	0.89	6.84-25	0.87	(3/4 T)
10	58.61	2.31-25 3.5%	1.79-25	0.81	1.78-25	0.80	Void Box
		Sulphur Activities					
8	39.01	1.08-24 5.5%	1.03-24	0.99	0.99-24	0.95	RPV (1/4 T)
9	49.61	1.46-25 5.9%	1.45-25	1.04	1.37-25	0.98	(3/4 T)
10	58.61	3.73-26 5.3%	3.70-26	1.03	3.51-26	0.98	Void Box

(1) Experimental results contain a contribution from the NESTOR core background. Calculated results refer only to the neutrons produced in the fission-plate for 1 Watt of NESTOR power. As indicated in ref. /1/, E values, in C/E ratios, are reduced by 4 % in the RPV and Void Box.

(*) Saturated activities are in units of reactions/(s.atom.NESTOR Watt). The effective threshold energies for the Indium and Sulphur detectors are respectively 1.30 and 2.8 MeV.

(**) Read as 3.93×10^{-24} (+/- 2.9%).

TAB. 5

SUMMARY OF MEASURED AND CALCULATED ^{103}Rh (n,n') ACTIVITIES (*)

ALONG THE NUCLEAR AXIS FOR THE PCA-REPLICA SLAB GEOMETRY BENCHMARK

Detec. Pos.	Dist. from Fiss. Plate (cm)	Measured (E) and Total Error (1 σ) (1)	JENDL-3.1 Natural Iron File		JENDL-3.1 Iron Files		Ref. Location
			Calculated (C) DOT 3.5-E (X,Y,Z) Synthesis	(1) C/E	Calculated (C) DOT 3.5-E (X,Y,Z) Synthesis	(1) C/E	
			Weighted Difference Model				
1	1.91	1.69-20 (**) 6.0%	1.42-20	0.86	1.41-20	0.85	
2	7.41	3.78-21 6.0%	3.37-21	0.91	3.38-21	0.91	12 cm Water Gap
3	12.41	1.40-21 6.0%	1.22-21	0.89	1.23-21	0.90	
4	14.01	1.27-21 6.0%	1.09-21	0.88	1.10-21	0.89	
5	19.91	4.23-22 6.0%	3.39-22	0.82	3.19-22	0.77	
6	25.41	1.15-22 7.0%	1.00-22	0.88	0.98-22	0.87	13 cm Water Gap
7	30.41	4.73-23 7.0%	4.06-23	0.88	3.97-23	0.86	
8	39.01	2.07-23 4.0%	1.93-23	0.97	1.83-23	0.92	RPV (1/4 T)
9	49.61	5.53-24 4.9%	5.33-24	1.00	4.41-24	0.83	(3/4 T)
10	58.61	1.80-24 4.6%	1.41-24	0.82	0.94-24	0.54	Void Box

(1) Experimental results contain a contribution from the NESTOR core background. Calculated results refer only to the neutrons produced in the fission-plate for 1 Watt of NESTOR power. As indicated in ref. /1/, E values, in C/E ratios, are reduced by 4 % in the RPV and Void Box and by 2 % in the water.

(*) Saturated activities are in units of reactions/(s.atom.NESTOR Watt). The effective threshold energy for the Rhodium detector is 0.69 MeV.

(**) Read as 1.69×10^{-20} (+/- 6.0%).

TAB. 6

SUMMARY OF MEASURED AND CALCULATED ^{115}In (n,n') AND ^{32}S (n,p) ACTIVITIES (*)

ALONG THE NUCLEAR AXIS FOR THE PCA-REPLICA SLAB GEOMETRY BENCHMARK

Detec. Pos.	Dist. from Fiss. Plate (cm)	(1) Measured (E) and Total Error (1 σ)	JENDL-3.1 Natural Iron File		JENDL-3.1 Iron Files		Ref. Location
			Calculated (C) DOT 3.5-E (X,Y,Z) Synthesis	(1) C/E	Calculated (C) DOT 3.5-E (X,Y,Z) Synthesis	(1) C/E	
			Weighted Difference Model				
			Indium Activities				
8	39.01	(**) 3.93-24 2.9%	3.55-24	0.94	3.34-24	0.89	RPV (1/4 T)
9	49.61	8.23-25 3.4%	7.03-25	0.89	5.87-25	0.74	(3/4 T)
10	58.61	2.31-25 3.5%	1.79-25	0.81	1.34-25	0.60	Void Box
			Sulphur Activities				
8	39.01	1.08-24 5.5%	1.03-24	0.99	1.01-24	0.97	RPV (1/4 T)
9	49.61	1.46-25 5.9%	1.45-25	1.04	1.42-25	1.01	(3/4 T)
10	58.61	3.73-26 5.3%	3.70-26	1.03	3.58-26	1.00	Void Box

(1) Experimental results contain a contribution from the NESTOR core background. Calculated results refer only to the neutrons produced in the fission-plate for 1 Watt of NESTOR power. As indicated in ref. /1/, E values, in C/E ratios, are reduced by 4 % in the RPV and Void Box.

(*) Saturated activities are in units of reactions/(s.atom.NESTOR Watt). The effective threshold energies for the Indium and Sulphur detectors are respectively 1.30 and 2.8 MeV.

(**) Read as 3.93×10^{-24} (+/- 2.9%).

FIGURES

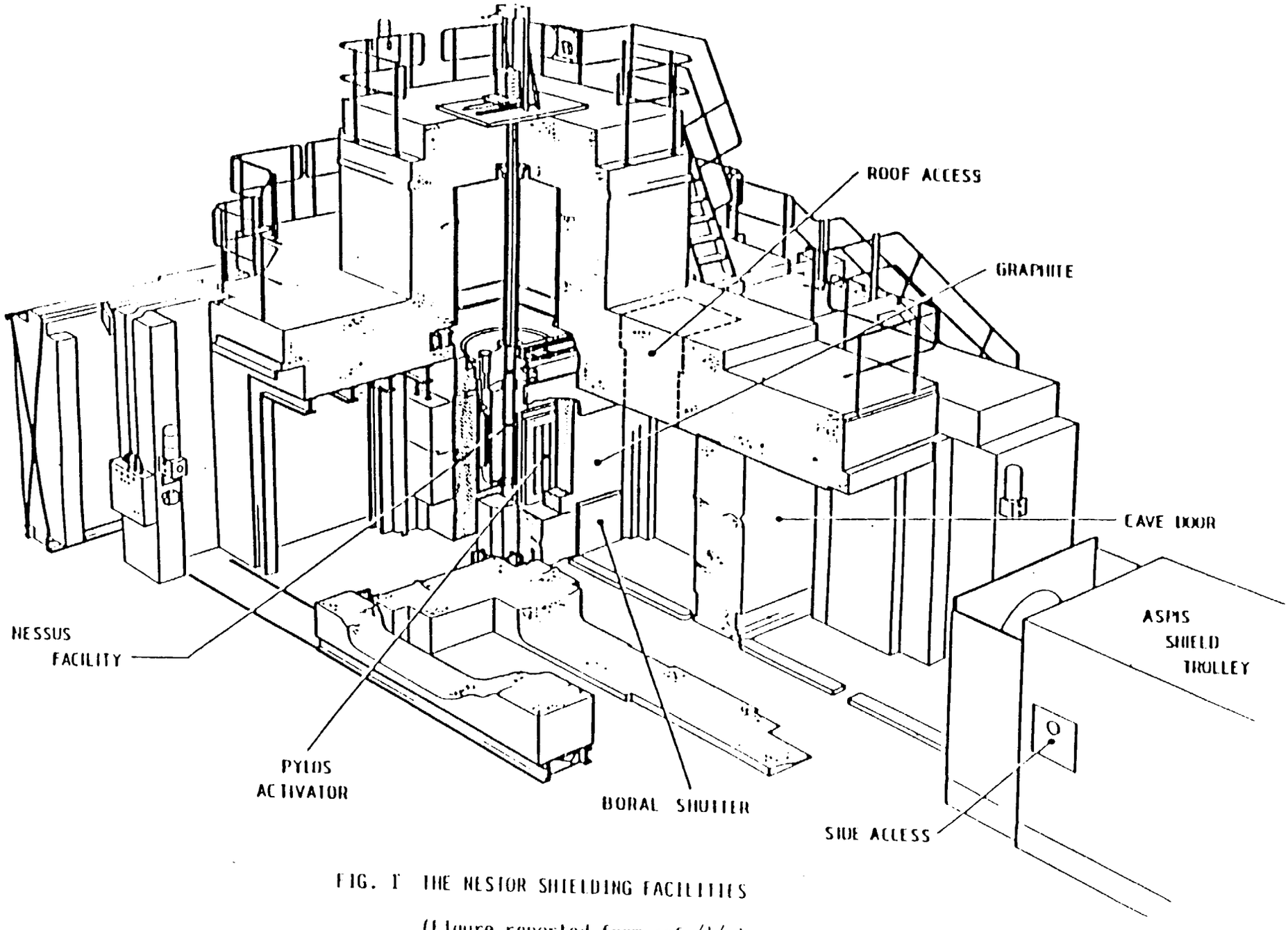

FIG. 1 THE NESTOR SHIELDING FACILITIES

(Figure reported from ref./1/)

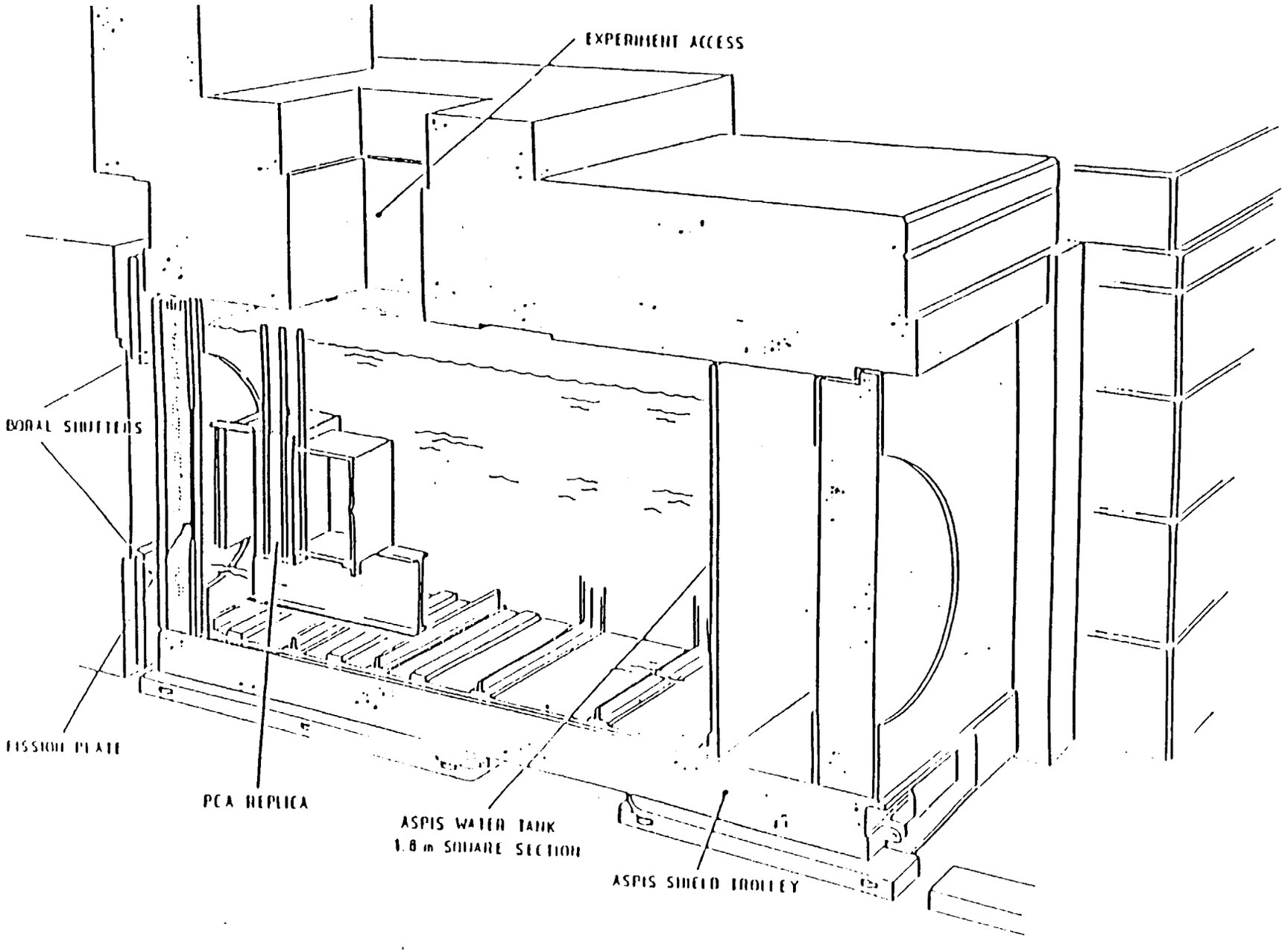

FIG. 2 THE PCA-REPLICA EXPERIMENT INSTALLED IN THE ASPIS SHIELD TROLLEY

(Figure reported from ref. /1/)

FIG. 3

LAYOUT OF THE 12/13 PCA-REPLICA CONFIGURATION FOR DOT 3.5-E CALCULATIONS

(Figure not to scale)

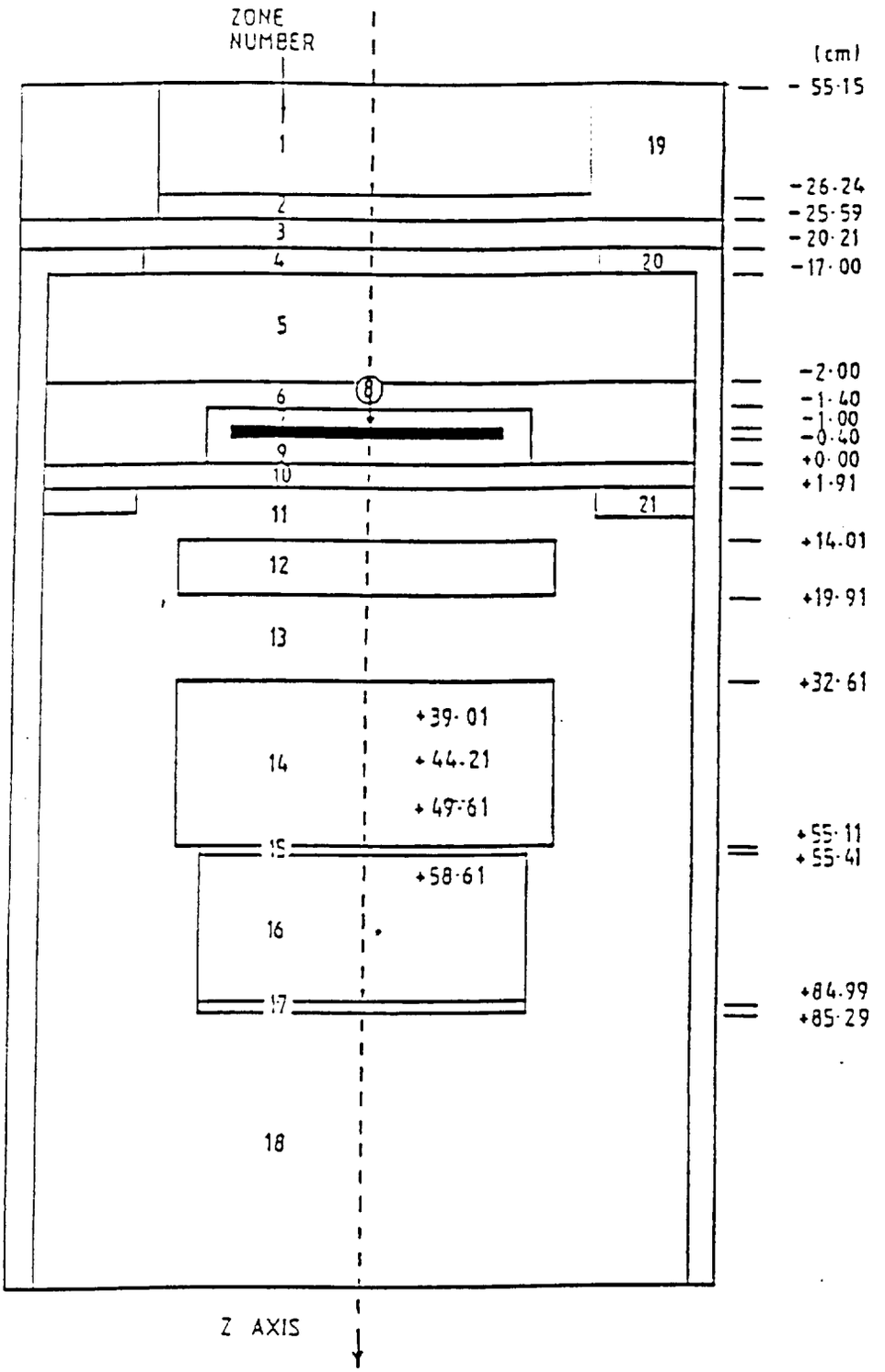

MATERIAL/ZONE NUMBER
Graphite: 1, 5.
Aluminium: 2, 4, 7, 8 (Fission Plate), 9, 10, 15, 17.
Void (Air): 3, 6, 16.
Water: 11, 13, 18.
Stainless Steel: 12.
Mild Steel: 14, 20, 21.
Concrete: 19.

FIG. 4

THE STANDARD COORDINATE SYSTEM

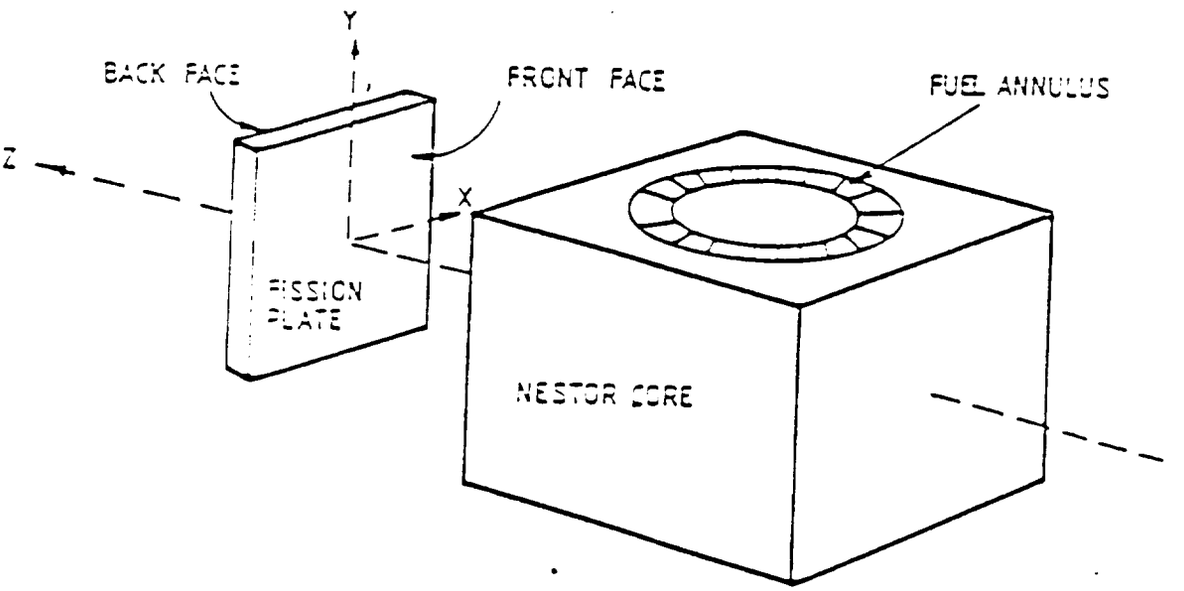

(Figure reported from ref./1/)

FIG. 5

REPLICA 12/13 Rh-103 (n,n') Rh-103m REACTION RATE RATIOS (CALCULATED / EXPERIMENTAL) ON THE HORIZONTAL AXIS

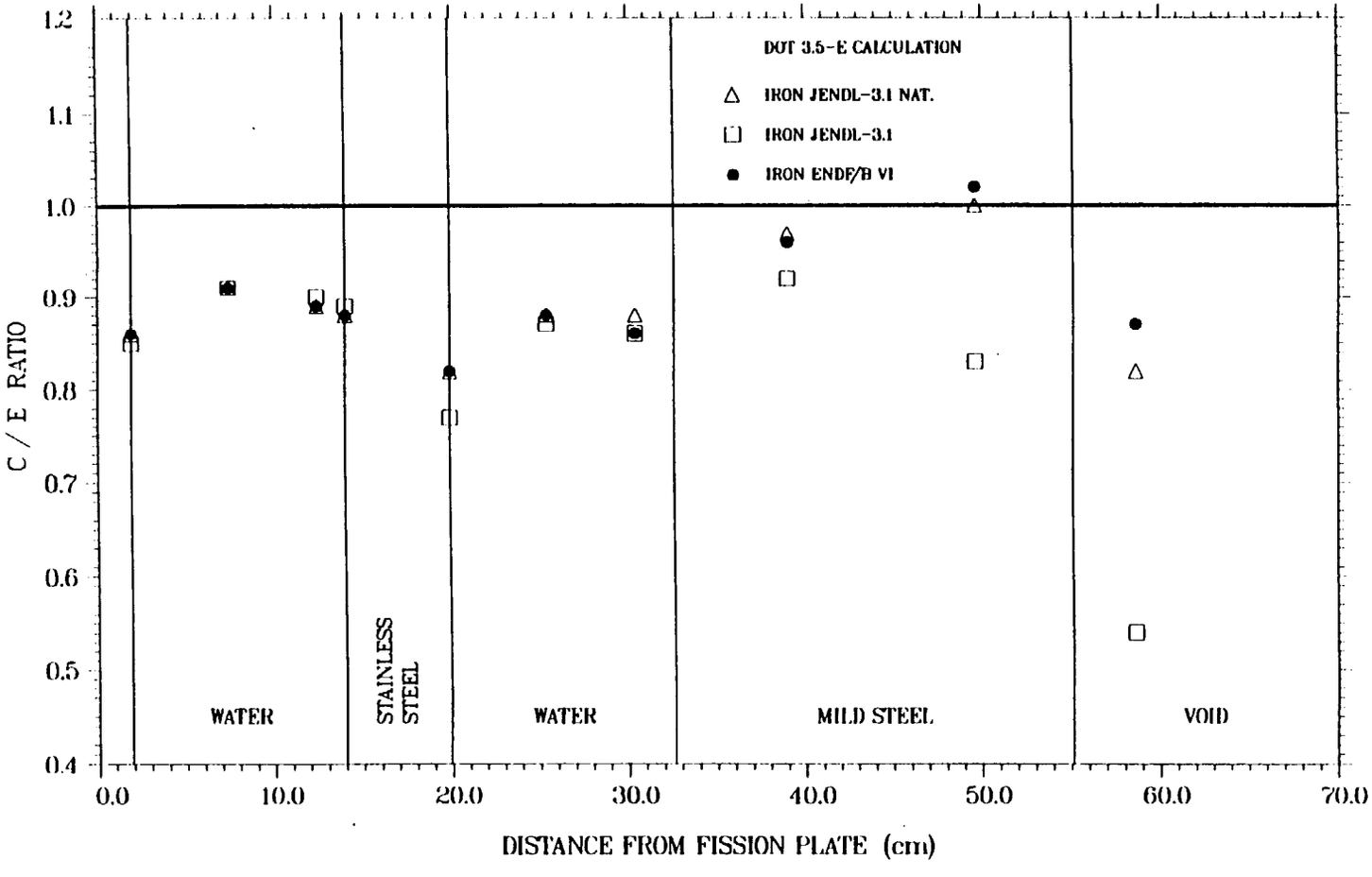

FIG. 6

REPLICA 12/13 In-115 (n,n') In-115m REACTION RATE RATIOS (CALCULATED / EXPERIMENTAL) ON THE HORIZONTAL AXIS

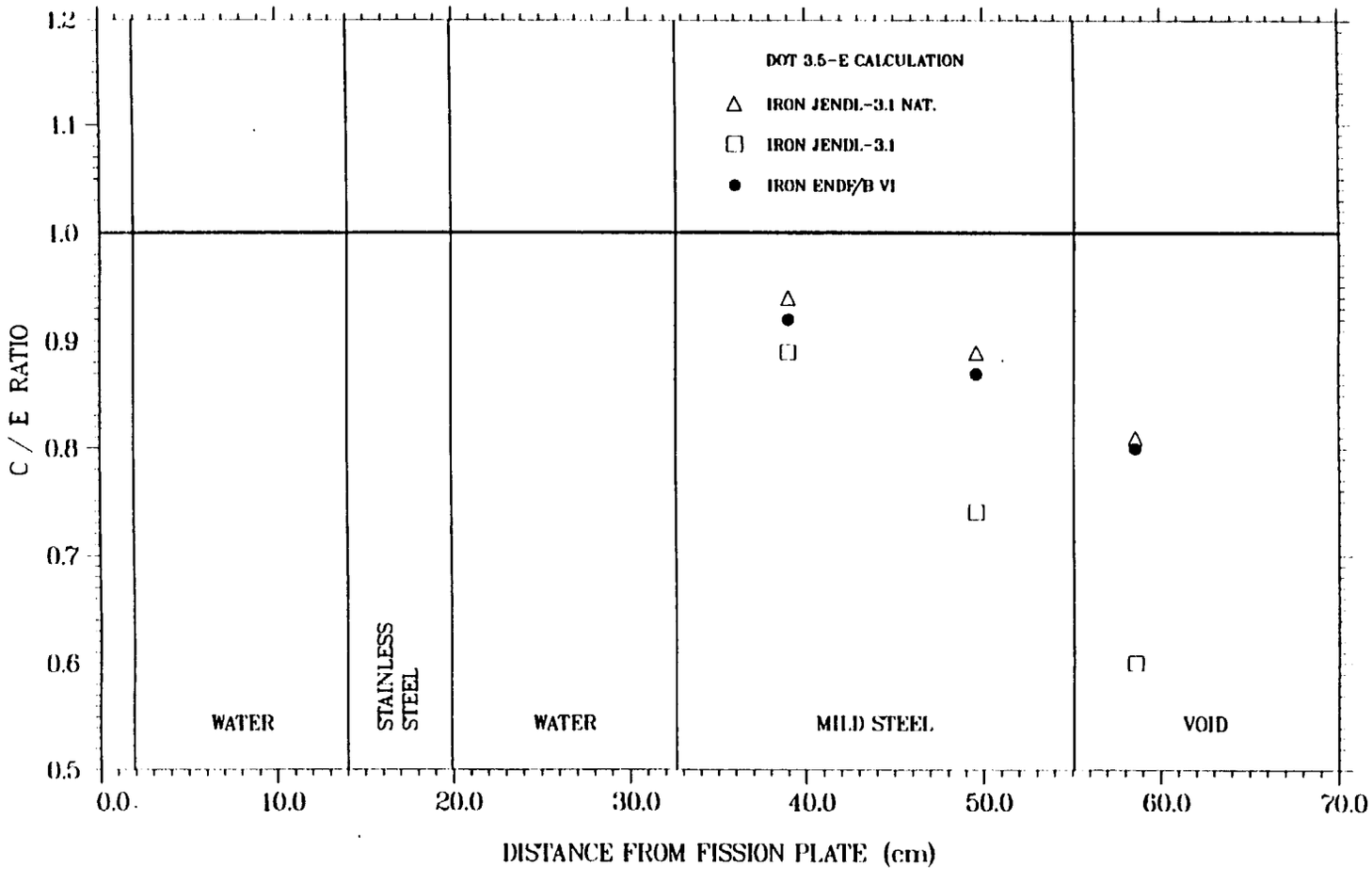

FIG. 7

REPLICA 12/13 S-32 (n,p) P-32 REACTION RATE RATIOS (CALCULATED / EXPERIMENTAL) ON THE HORIZONTAL AXIS

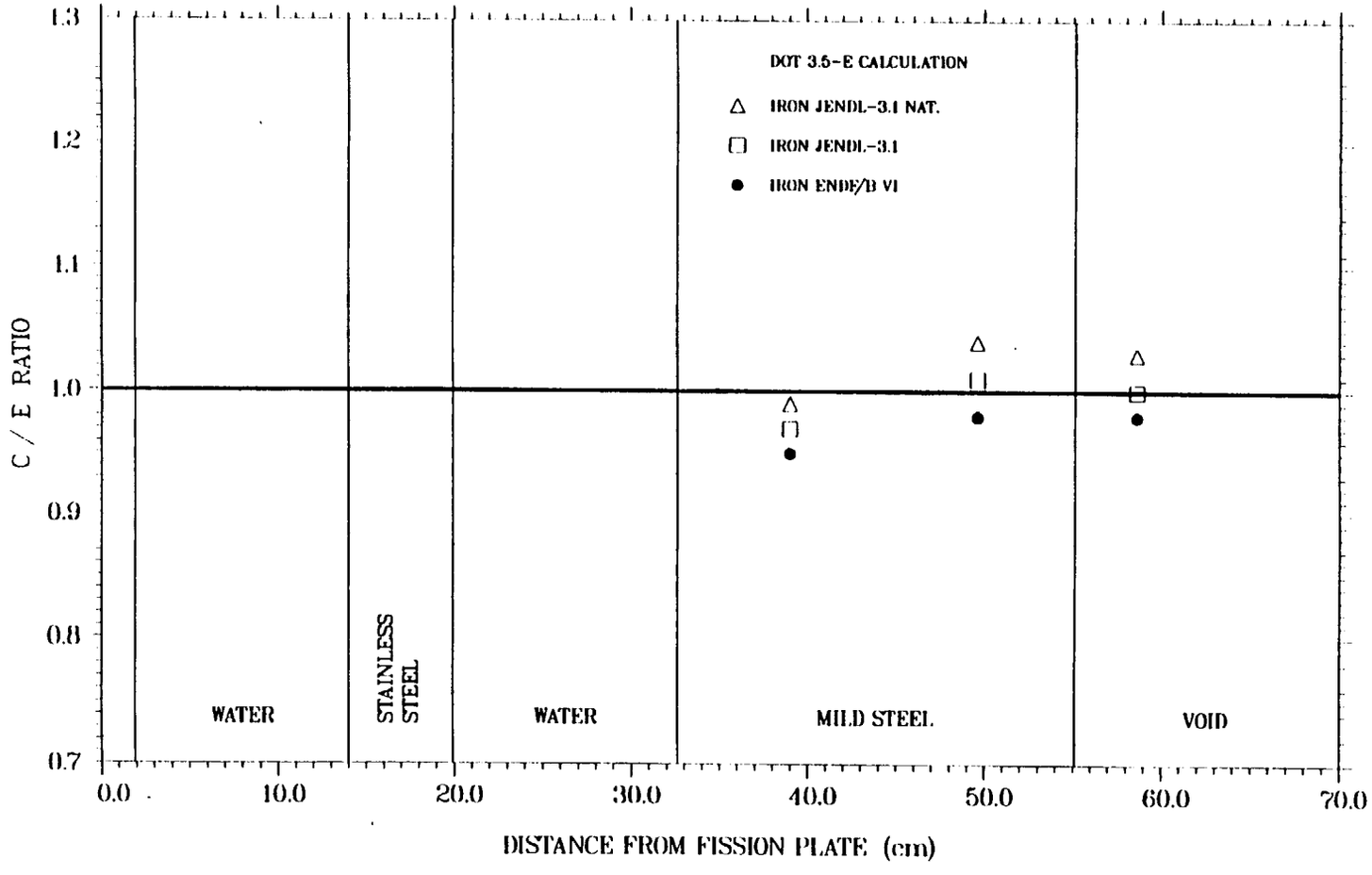

FIG. 8

REPLICA 12/13 SPECTRUM IN THE RPV T/4 POSITION (MILD STEEL)

COMPARISON OF MEASUREMENT AND CALCULATION

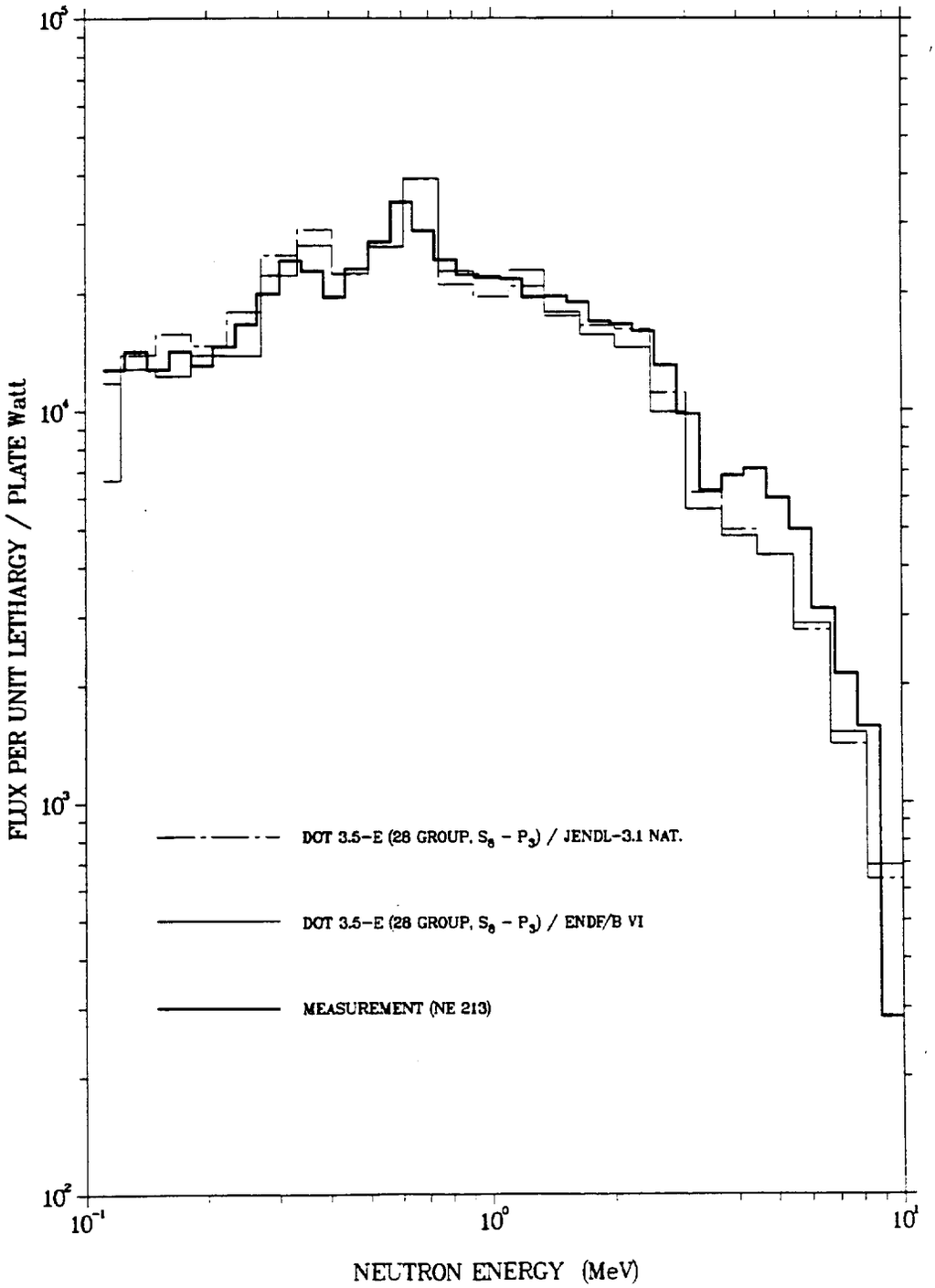

FIG. 9

REPLICA 12/13 RPV T/4 POSITION (MILD STEEL)

RATIO OF THE JENDL-3.1 NAT. TO THE ENDF/B VI GROUP FLUXES

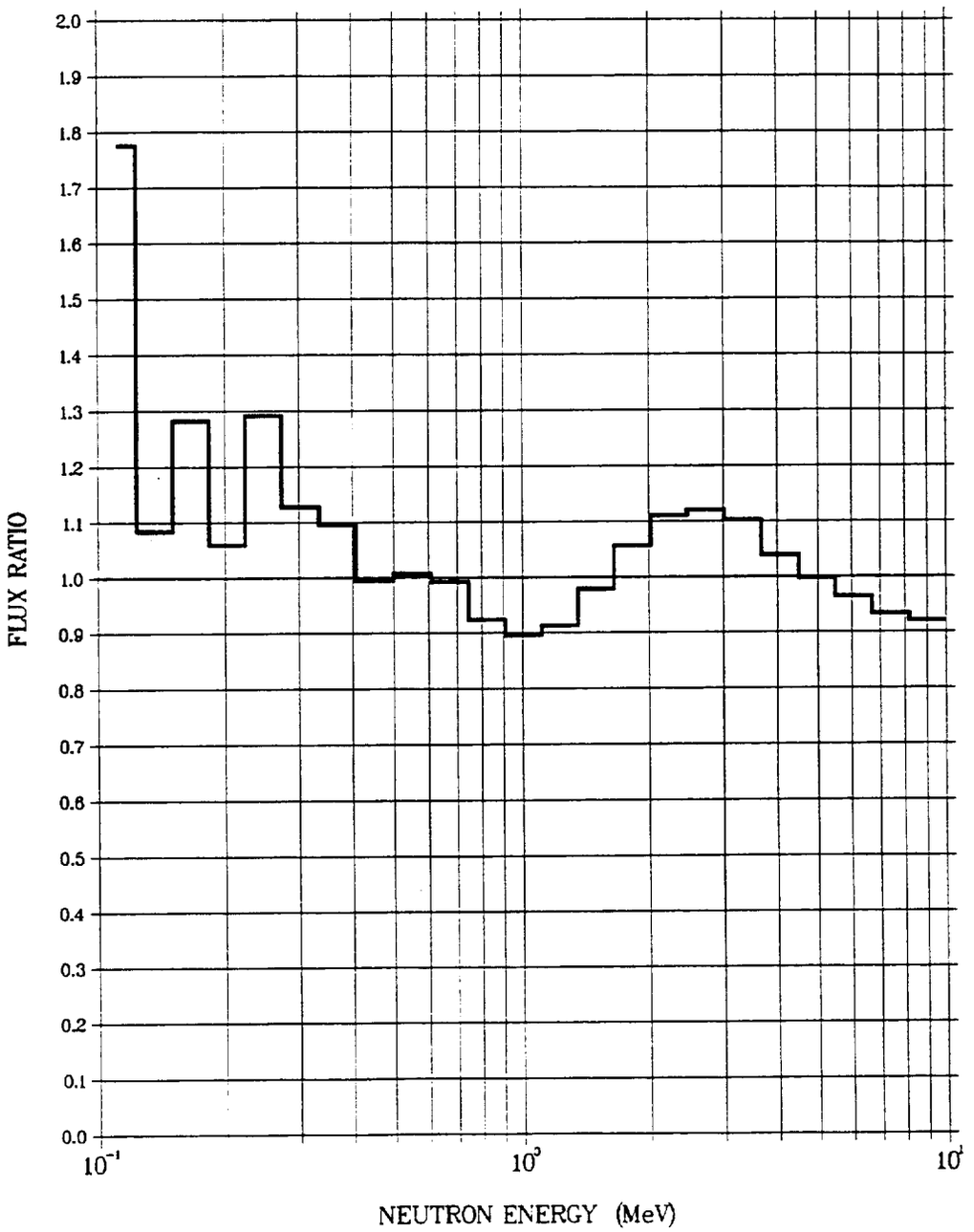

FIG. 10

REPLICA 12/13 SPECTRUM IN THE VOID BOX POSITION (AIR)

COMPARISON OF MEASUREMENT AND CALCULATION

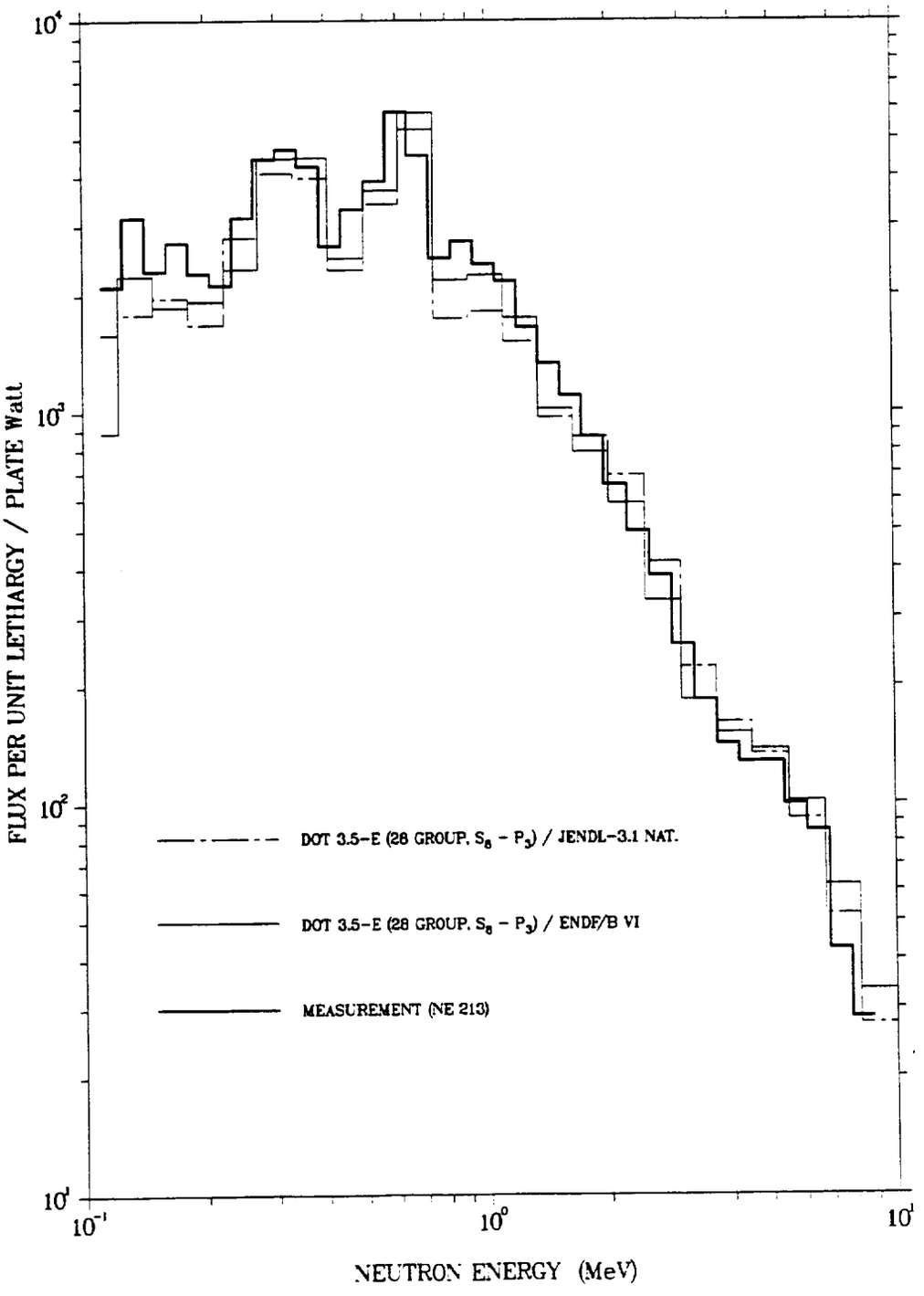

FIG. 11

REPLICA 12/13 VOID BOX POSITION (AIR)

RATIO OF THE JENDL-3.1 NAT. TO THE ENDF/B VI GROUP FLUXES

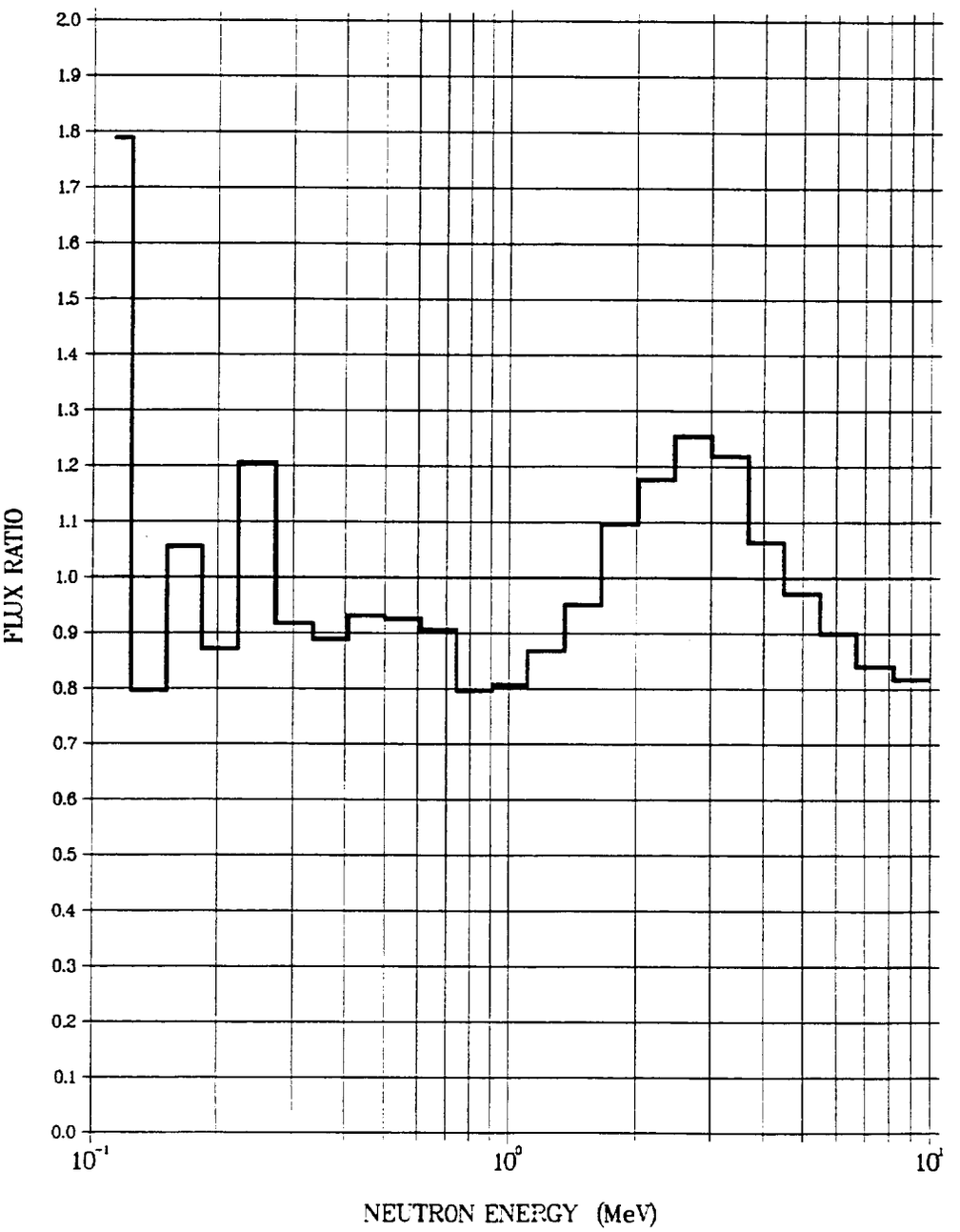

FIG. 12

REPLICA 12/13 SPECTRUM IN THE RPV T/4 POSITION (MILD STEEL)

COMPARISON OF MEASUREMENT AND CALCULATION

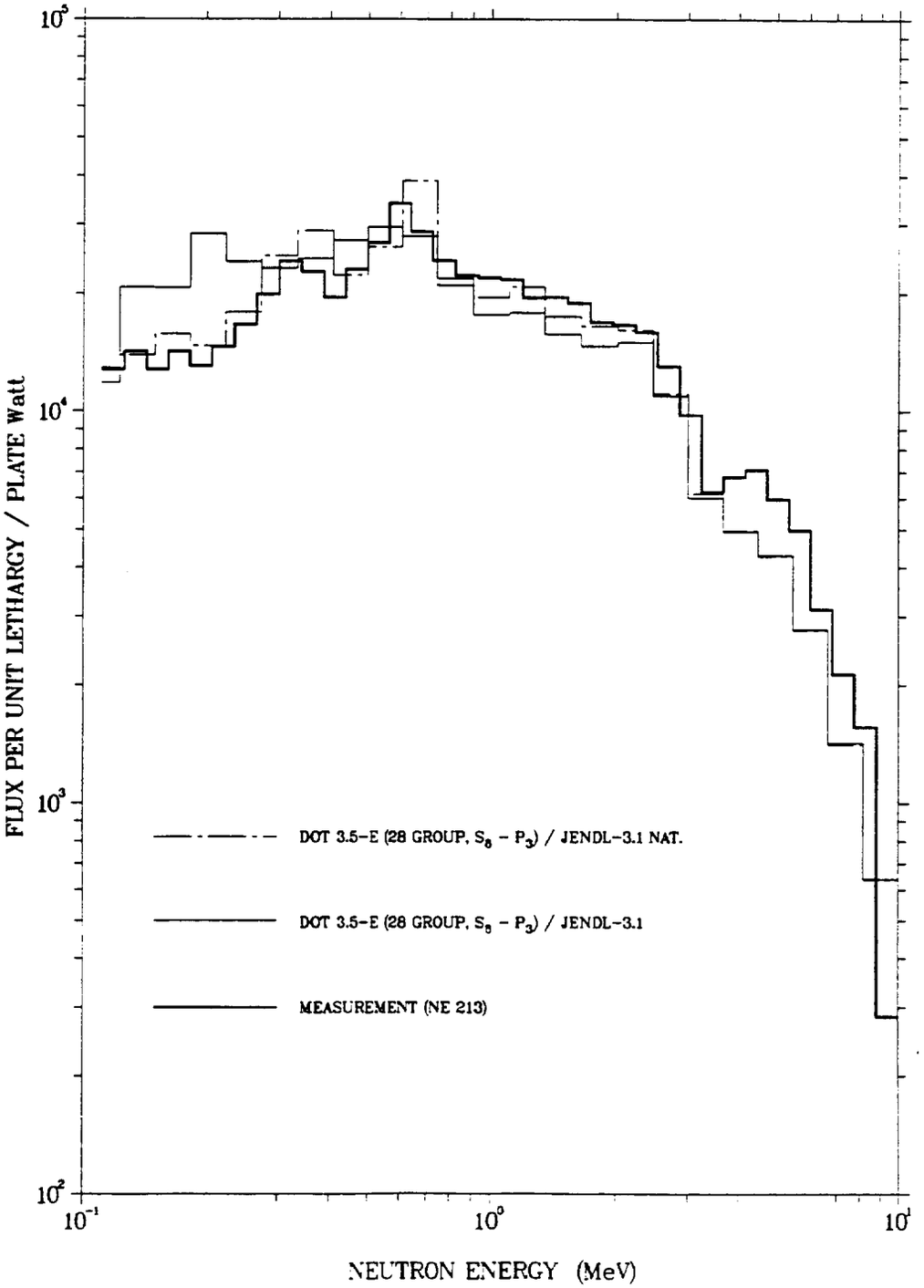

FIG. 13

REPLICA 12/13 RPV T/4 POSITION (MILD STEEL)

RATIO OF THE JENDL-3.1 TO THE JENDL-3.1 NAT. GROUP FLUXES

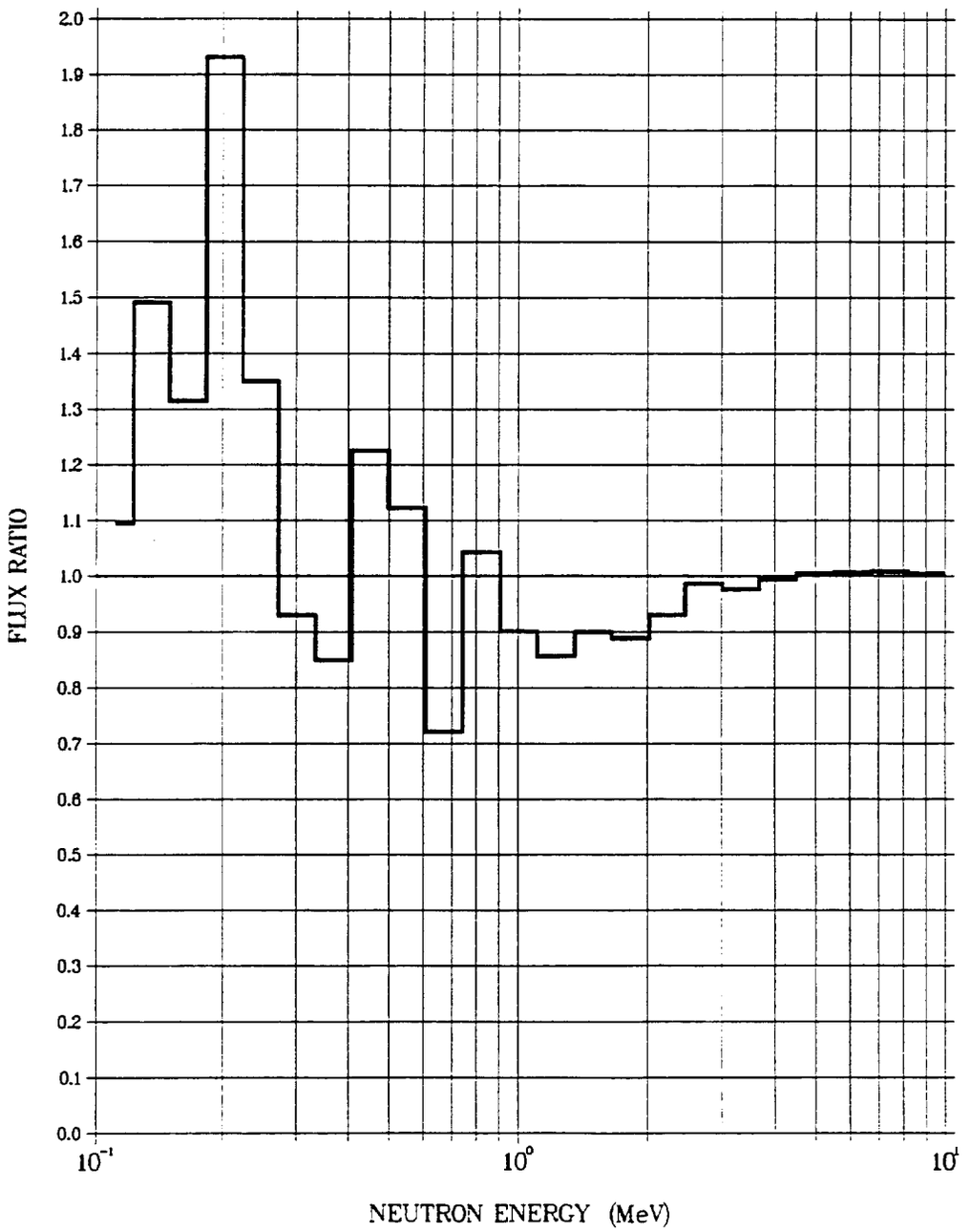

FIG. 14

REPLICA 12/13 SPECTRUM IN THE VOID BOX POSITION (AIR)

COMPARISON OF MEASUREMENT AND CALCULATION

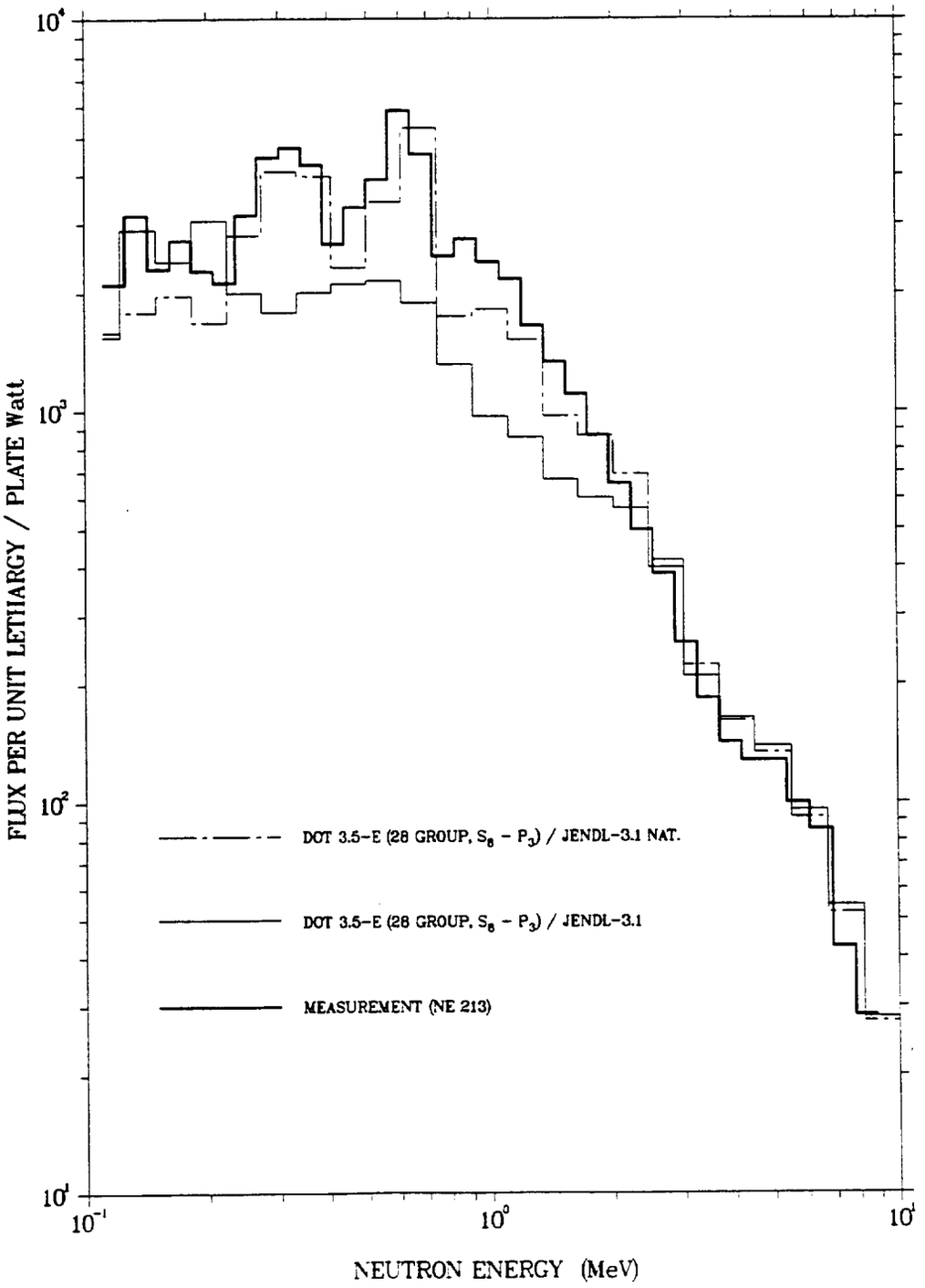

FIG. 15

REPLICA 12/13 VOID BOX POSITION (AIR)

RATIO OF THE JENDL-3.1 TO THE JENDL-3.1 NAT. GROUP FLUXES

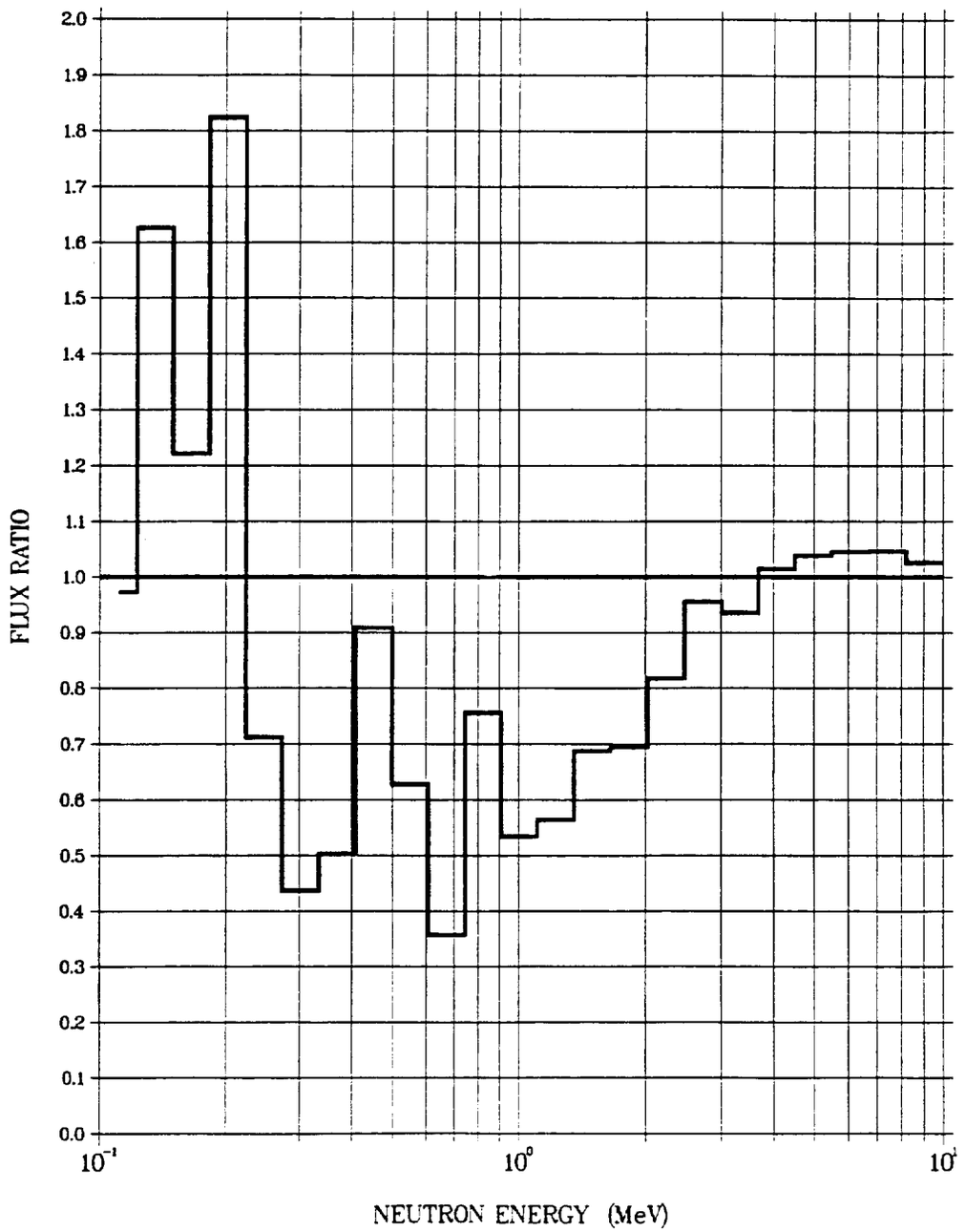

FIG. 16

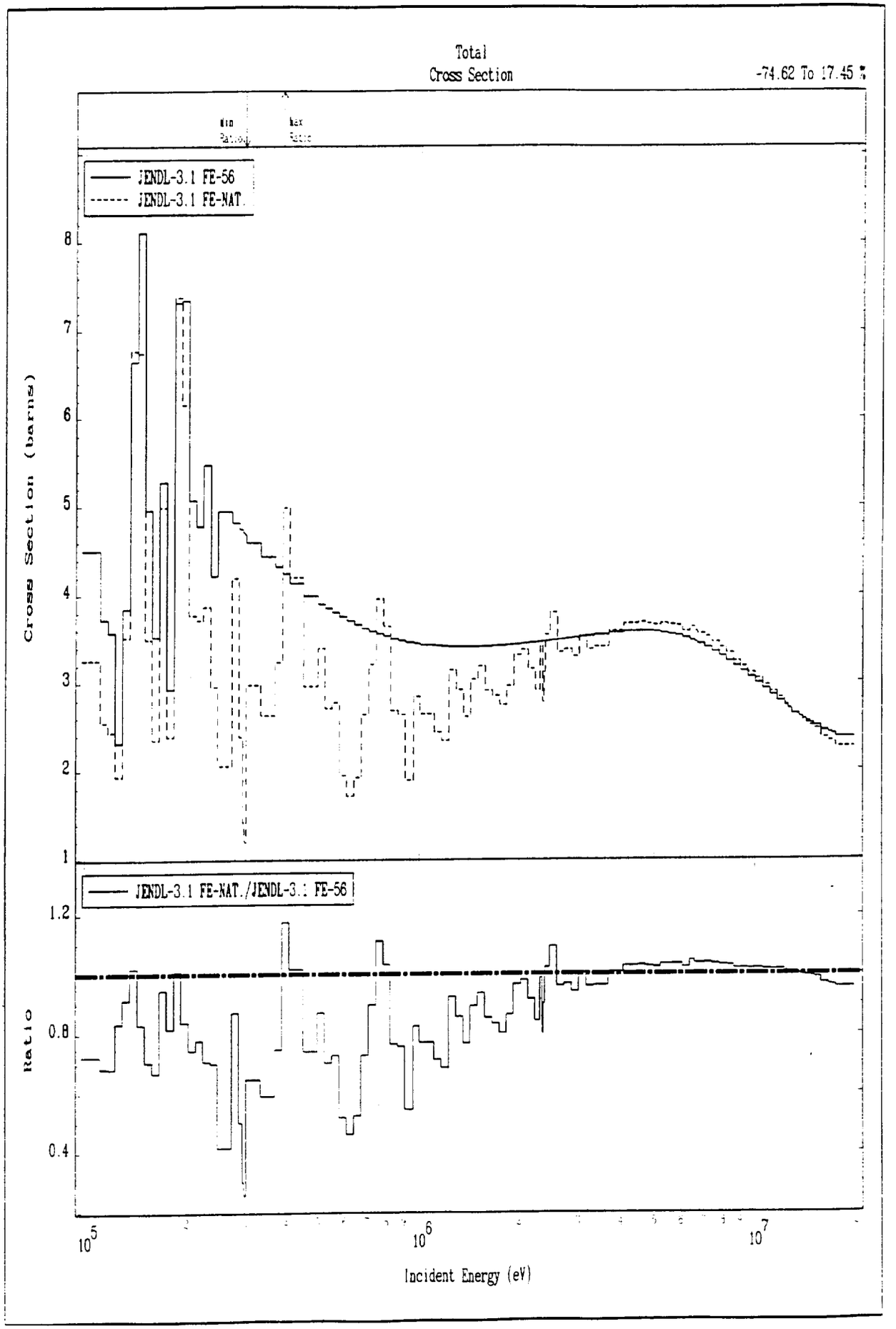
Total
Cross Section
-74.62 To 17.45 %
JENDL-3.1 FE-56
JENDL-3.1 FE-NAT.
Cross Section (barns)
8
7
6
5
4
3
2
1
JENDL-3.1 FE-NAT./JENDL-3.1 FE-56
Ratio
1.2
0.8
0.4
10^5
10^6
10^7
Incident Energy (eV)

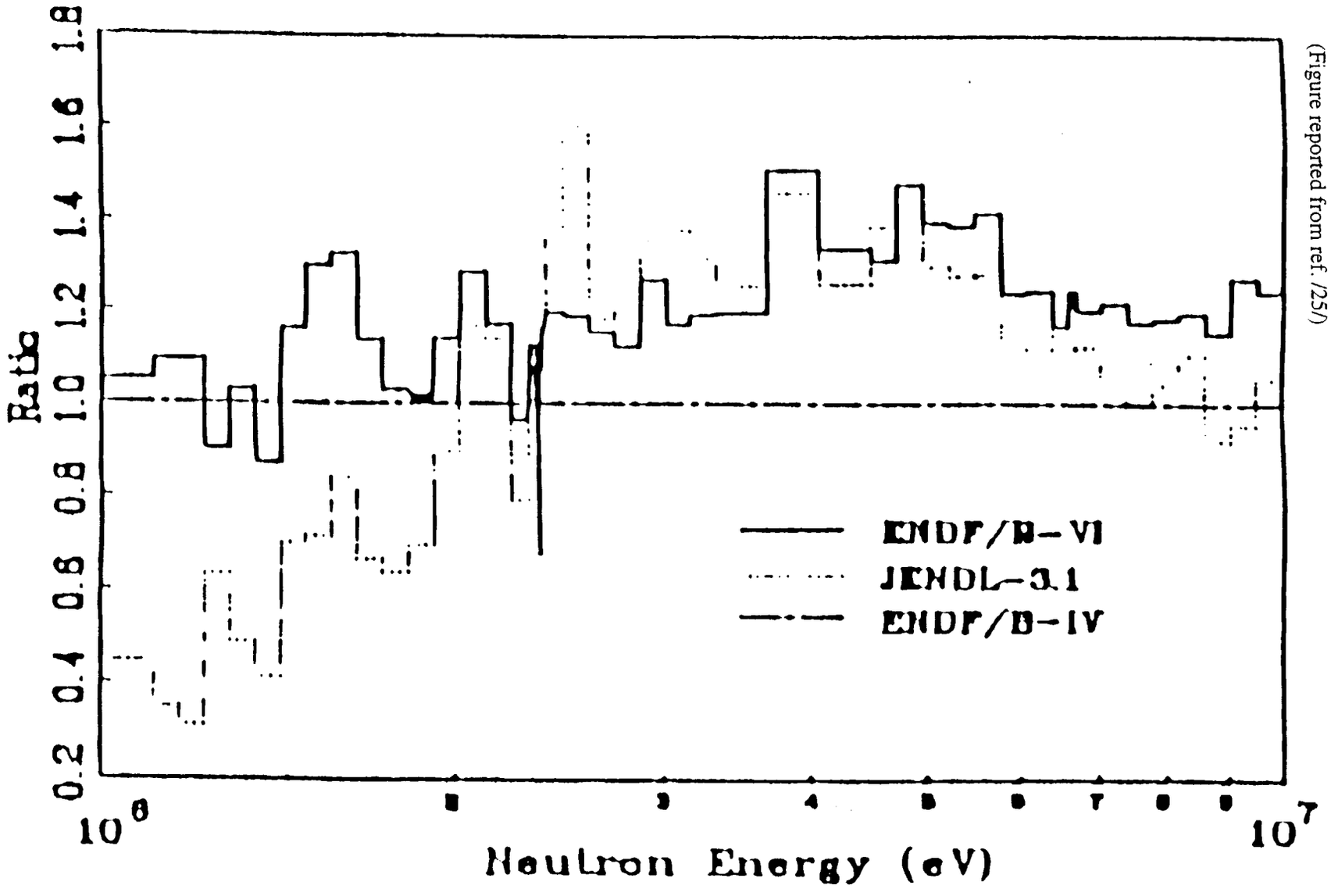

(Figure reported from ref. /25/)

FIG. 17 Ratio of Flux above 1 MeV Calculated by MCNP with different Iron Evaluations to Result with ENDF/B-IV in the Cavity.

FIG. 18

REPLICA 12/13 VOID BOX POSITION (AIR)

RATIO OF THE JENDL-3.1 TO THE ENDF/B VI GROUP FLUXES

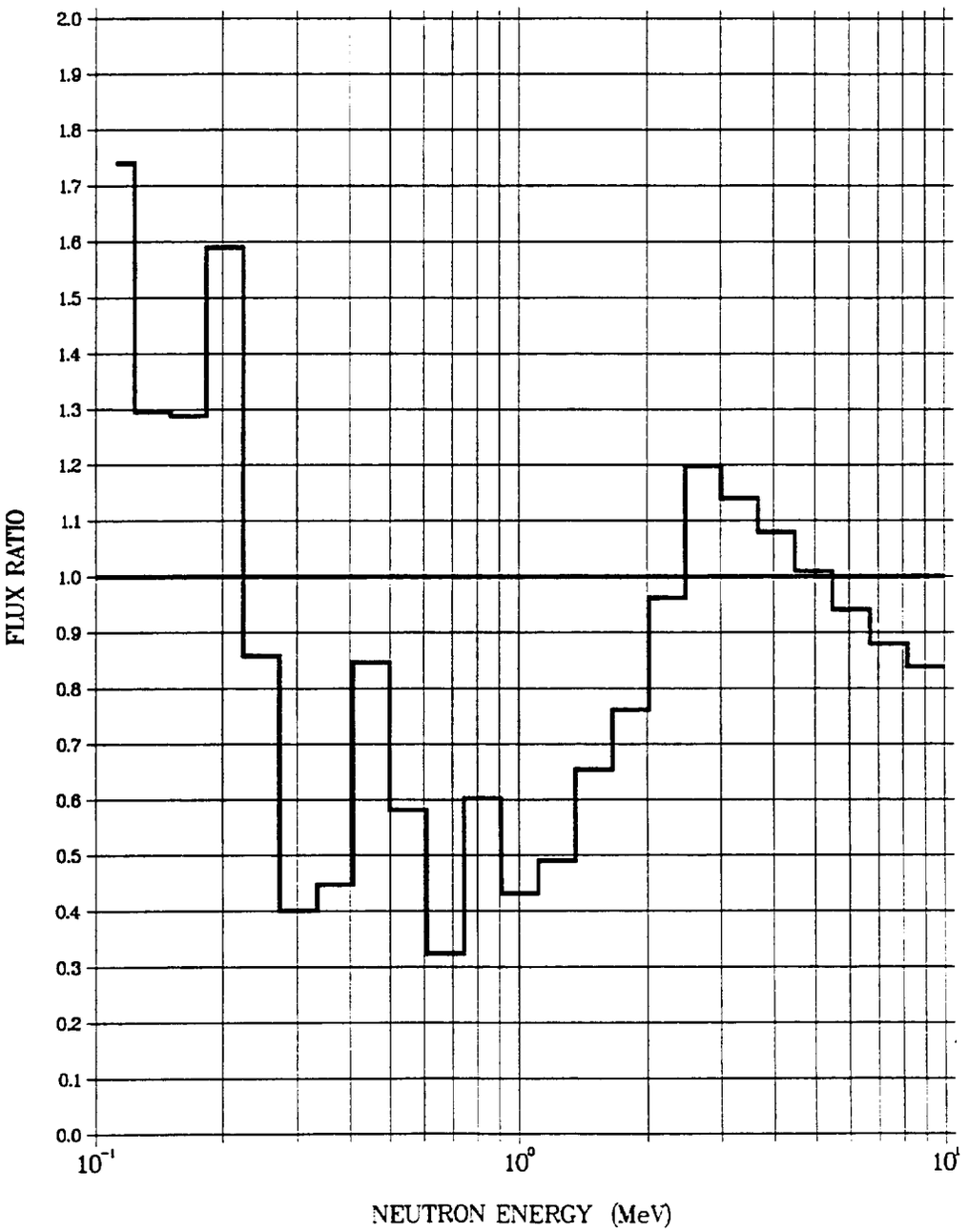

FIG. 19

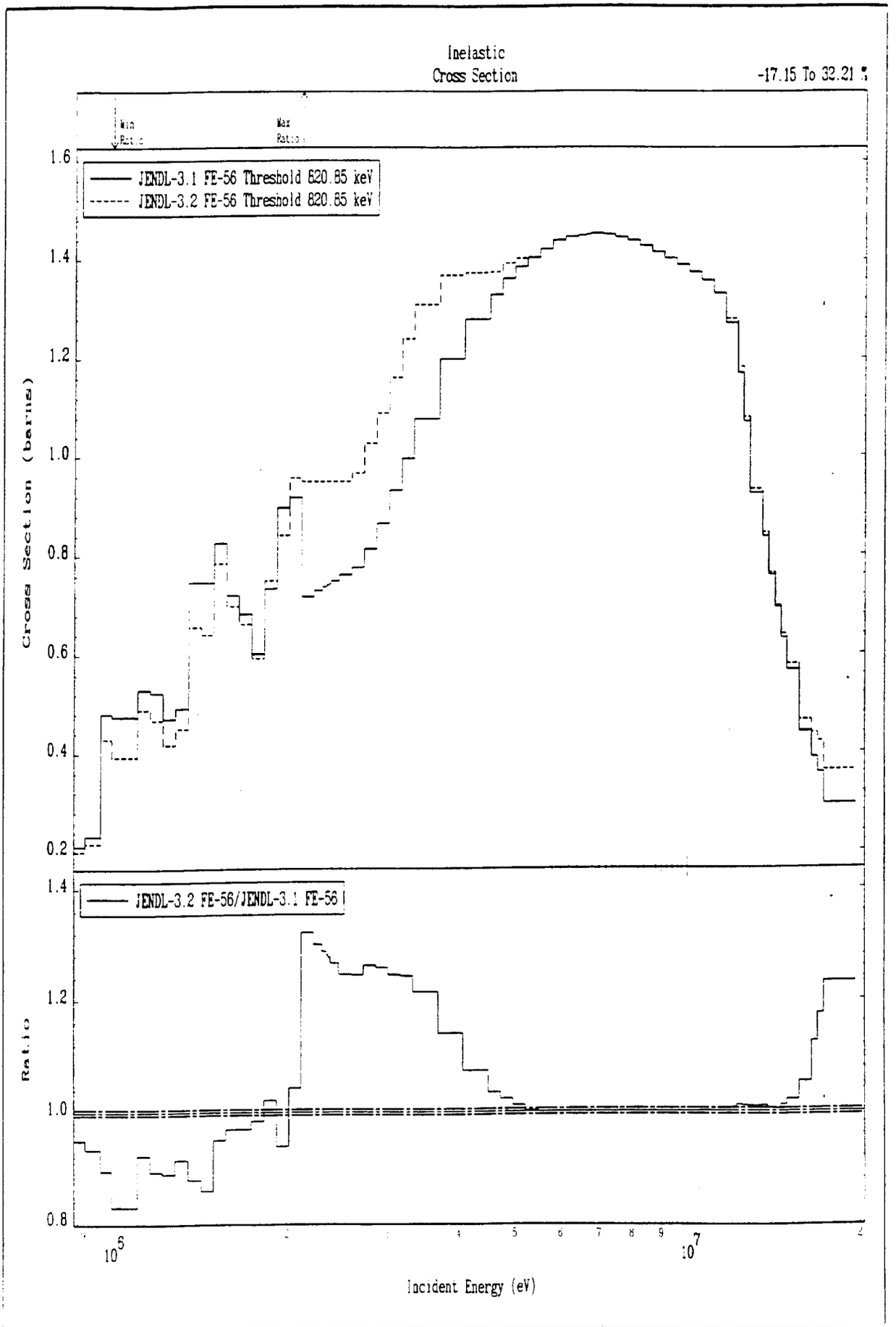
Inelastic
Cross Section
-17.15 To 32.21 %
JENDL-3.1 FE-56 Threshold 820.85 keV
JENDL-3.2 FE-56 Threshold 820.85 keV
Cross Section (barns)
1.6
1.4
1.2
1.0
0.8
0.6
0.4
0.2
JENDL-3.2 FE-56/JENDL-3.1 FE-56
Ratio
1.4
1.2
1.0
0.8
10^5
10^7
Incident Energy (eV)

FIG. 20

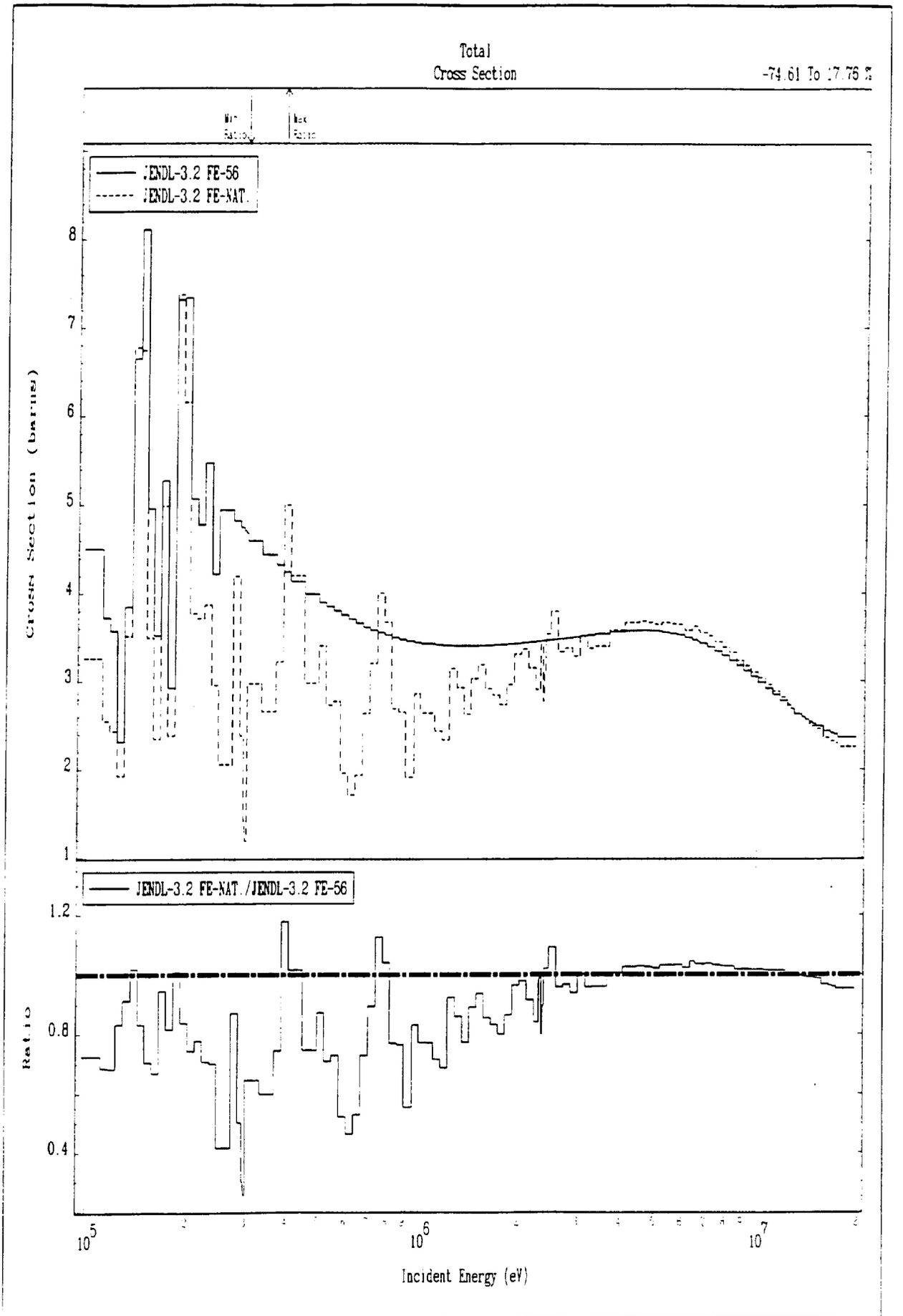
Total
Cross Section
-74.61 To 17.76 %
JENDL-3.2 FE-56
JENDL-3.2 FE-NAT.
Cross Section (barns)
JENDL-3.2 FE-NAT./JENDL-3.2 FE-56
Ratio
Incident Energy (eV)

FIG. 21

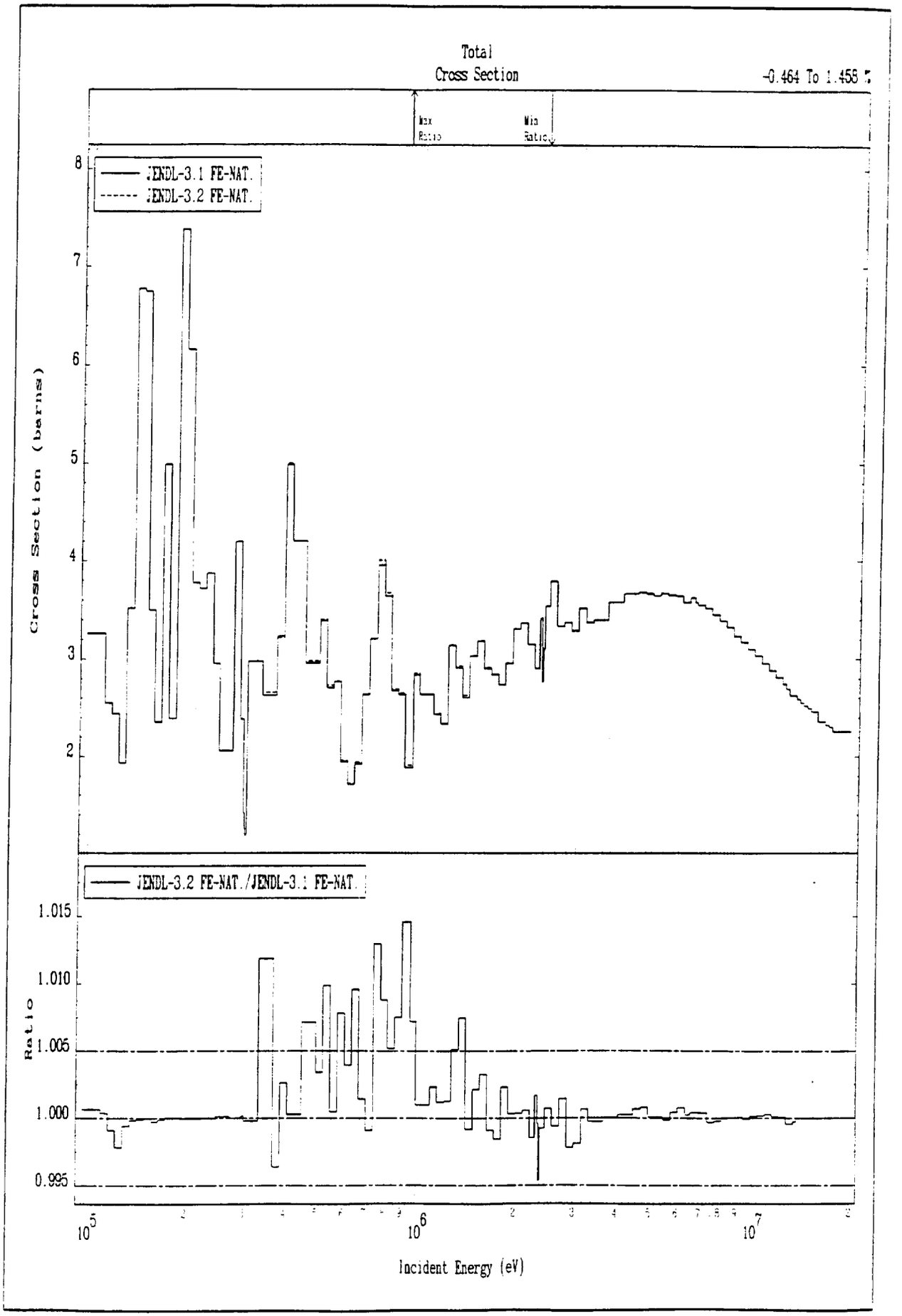
Total
Cross Section
-0.464 To 1.458 7
Max Ratio
Min Ratio
JENDL-3.1 FE-NAT.
JENDL-3.2 FE-NAT.
Cross Section (barns)
8
7
6
5
4
3
2
JENDL-3.2 FE-NAT./JENDL-3.1 FE-NAT.
Ratio
1.015
1.010
1.005
1.000
0.995
10^5
10^6
10^7
Incident Energy (eV)

Edito dall' ENEA
Unità Comunicazione e Informazione
Lungotevere Grande Ammiraglio Thaon di Revel, 76 - 00196 Roma
Stampa: COM-Centro Stampa Tecnografico - C. R. Frascati

Finito di stampare nel mese di marzo 1997